

1

2 ***Plasmodium falciparum* protein Pfs16 is a target for transmission-**
3 **blocking antimalarial drug development**

4

5 Sabrina Yahiya¹, Charlie N. Saunders^{1,2}, Ursula Straschil¹, Oliver J. Fischer², Ainoa Rueda-
6 Zubiaurre², Silvia Haase¹, Gema Vizcay-Barrena³, Sarah Jordan¹, Sarah Hassan², Michael J.
7 Delves¹, Edward W. Tate², Anna Barnard², Matthew J. Fuchter² & Jake Baum^{1*}

8

9 ¹ Department of Life Sciences, Imperial College London, Sir Alexander Fleming Building, Exhibition
10 Road, South Kensington, London, SW7 2AZ, UK.

11 ² Department of Chemistry, Imperial College London, Molecular Sciences Research Hub, White
12 City Campus, Wood Lane, London, W12 0BZ, UK.

13 ³ Centre for Ultrastructural Imaging, New Hunt's House, Guy's Campus, King's College London,
14 London, SE1 1UL, UK.

15

16 ***Correspondence to:**

17 Jake Baum (jake.baum@imperial.ac.uk), Department of Life Sciences, Imperial College London,
18 Exhibition Road, South Kensington, London SW7 2AZ, United Kingdom.

19 **Key words**

20 *Plasmodium falciparum*; malaria; high throughput screening; target identification; target validation;
21 transmission; drug discovery; exflagellation; gametocytes; gametogenesis.

22 **Running Title:** Pfs16 a transmission-blocking antimalarial target

23 **ABSTRACT**

24 Phenotypic cell-based screens are critical to the discovery of new antimalarial lead compounds.
25 However, identification and validation of cellular targets of lead compounds is required following
26 discovery in a phenotypic screen. We recently discovered a *Plasmodium* transmission-blocking N-
27 ((4-hydroxychroman-4-yl)methyl)-sulfonamide (N-4HCS) compound, **DDD01035881**, in a
28 phenotypic screen. **DDD01035881** and its potent derivatives have been shown to block
29 *Plasmodium* male gamete formation (microgametogenesis) with nanomolar activity. Here, we
30 synthesised a photoactivatable N-4HCS derivative, probe **2**, to identify the N-4HCS cellular target.
31 Using probe **2** in photo-affinity labelling coupled with mass spectrometry, we identified the 16 kDa
32 *Plasmodium falciparum* parasitophorous vacuole membrane protein Pfs16 as the likely cellular
33 target of the N-4HCS series. Further validating Pfs16 as the cellular target of the N-4HCS series,
34 the Cellular Thermal Shift Assay (CETSA) confirmed DDD01035881 stabilised Pfs16 in lysate from
35 activated mature gametocytes. Additionally, photo-affinity labelling combined with in-gel
36 fluorescence and immunoblot analysis confirmed the N-4HCS series interacted with Pfs16. High-
37 resolution, widefield fluorescence and electron microscopy of N-4HCS-inhibited parasites was
38 found to result in a cell morphology entirely consistent with targeted gene disruption of *Pfs16*.
39 Taken together, these data strongly implicate Pfs16 as the target of **DDD01035881** and establish
40 the N-4HCS scaffold family as a powerful starting point from which future transmission-blocking
41 antimalarials can be developed.

42 INTRODUCTION

43 Malaria continues to devastate millions, with 228 million cases and 405,000 deaths from malaria
44 reported in 2018 alone¹. The causative agent of malaria, the protozoan *Plasmodium* parasite,
45 transitions between a mammalian host and *Anopheles* mosquito vector, demonstrating extensive
46 cellular plasticity in form across the different lifecycle stages². Symptomatic stages of *Plasmodium*
47 are restricted to the asexual blood stages and can be targeted and rapidly killed by current frontline
48 antimalarials, including artemisinin and its derivatives³. Sexual forms (male and female
49 gametocytes) are relatively dormant in the blood and generally more resistant to the effects of
50 conventional antimalarials, yet they are entirely responsible for human to mosquito transmission⁴.

51 Although huge gains have been made in reducing the burden of malaria since the turn of the
52 millennium, current control measures are threatened by the emergence and spread of parasite
53 resistance to artemisinin-based combination therapies along with mosquito resistance to
54 insecticides¹. To combat rising parasite resistance, new antimalarial drugs with alternative modes
55 of action are critically needed³. Transmission of the parasite from human to mosquito is one of the
56 major bottlenecks in the parasite lifecycle⁵. Given the necessity of transmission to the *Plasmodium*
57 life cycle and proven capacity of transmission-blocking interventions to effectively break the cycle⁶,
58 the process of transmission is emerging as a key target for future antimalarial drug development⁷.
59 A primary target for transmission interventions is the dormant circulating gametocyte, responsible
60 for onwards *Plasmodium* transmission. Drugs that either kill or sterilize these forms in the human
61 host, or prevent fertilisation of resulting gametes in the mosquito gut, would theoretically block
62 transmission⁸. Currently, however, the only approved antimalarials with defined transmission
63 blocking activity are primaquine and tafenoquine of the 8-aminoquinoline family. Use of primaquine
64 is impeded by its clinical safety; the drug being associated with haemolysis in G6PD-deficient
65 patients⁹. New drugs that target the transmission process could therefore have substantial impact
66 in malaria control.

67 The male and female gametocytes of *P. falciparum* are recognised by their characteristic falciform
68 shape. Gametocytes maintain quiescence as they mature over five distinct morphological stages in
69 the human host, sequestering in the bone marrow and spleen until reaching maturity¹⁰. Upon

70 reaching maturity, stage V gametocytes re-enter the host circulation where they are available for
71 transmission to *Anopheles* mosquito vectors during a bloodmeal. The formation of gametes from
72 gametocytes, or gametogenesis, occurs in the mosquito midgut. During gametogenesis, male
73 gametocytes transform to 8 haploid male/microgametes (microgametogenesis) whilst female
74 gametocytes form a single haploid female/macrogamete (macrogametogenesis)^{11,12}. While females
75 undergo a relatively simple rounding up and erythrocyte egress process, formation of male
76 gametes during microgametogenesis is a notably complex and rapid process. The process
77 involves simultaneous egress from host erythrocytes, three rounds of DNA replication alternating
78 with endomitotic division and eventual formation of axonemes^{11,12}. Axonemes, which nucleate from
79 basal bodies, emerge from the parental cell as haploid microgametes in the process of
80 exflagellation. Fertilisation between male and female gametes gives rise to a diploid zygote that,
81 following mosquito midgut colonization, eventually yields haploid motile sporozoites responsible for
82 the next transmission cycle to humans².

83 Efforts to identify novel drugs targeting processes from symptomatic blood through to transmission
84 have been significantly bolstered by advances in high throughput phenotypic screening of
85 compound libraries⁷. However, whilst phenotypic screens supersede target-based drug discovery
86 in their ability to rapidly identify hits, the lack of knowledge on the hit target or its mode of action
87 can result a lengthy process of development or safety concerns during clinical testing. Elucidation
88 of a hit compound's cellular target(s) and mode of action prior to clinical testing is therefore
89 essential for improving the success rates of drug candidates¹³. One recent exemplar high
90 throughput screen involved testing of a large diverse chemical library (the Global Health Chemical
91 Diversity Library (GHCDL)) against both transmissible and symptomatic stages of *Plasmodium*.
92 The GHCDL screen identified hits with diverse activity profiles against the *Plasmodium* lifecycle,
93 including hits with multistage, transmission-specific, sex-specific and stage-specific activity¹⁴.
94 Within the library, a series of compounds with an N-((4-hydroxychroman-4-yl)methyl)-sulfonamide
95 (N-4HCS) scaffold were found to potently inhibit formation of *Plasmodium* male gametes from
96 mature stage V male gametocytes. The most potent hit from this scaffold series, **DDD01035881**,
97 has since been extensively studied by structure activity relationship, yielding hits with half maximal

98 inhibitory (IC₅₀) concentrations in the nanomolar range¹⁵. Importantly, **DDD01035881** and
99 derivatives were also shown to have minimal impact on viability of HepG2 mammalian cells,
100 suggesting they have low toxicity¹⁵.

101 To advance the N-4HCS scaffold here we sought to identify the mode of action and/or cellular
102 target of **DDD01035881**. Using photo affinity labelling, label-free Cellular Thermal Shift Assay
103 (CETSA) and cellular analysis of treated parasites, we present strong interdisciplinary evidence
104 that the target of **DDD01035881** and N-4HCS scaffold is the *Plasmodium falciparum* 16 kDa
105 parasitophorous vacuole membrane protein, Pfs16. Given the power of transmission blocking
106 therapeutics and drive for discovery of further, novel combination therapies, these data suggest the
107 N-4HCS scaffold may be an excellent foundation for future antimalarial treatment or preventative
108 regimens and positions Pfs16 as a novel target for further development.

109 RESULTS

110 The N-4HCS scaffold was recently identified in a high-throughput screen for transmission blocking
111 antimalarials¹⁴, with subsequent development to improve its activity by medicinal chemistry¹⁵. We
112 sought to determine a potential mode of action and cellular target for the N-4HCS scaffold, starting
113 out from the original hit **DDD01035881**, given its potency for inhibiting *Plasmodium falciparum*
114 parasite microgametogenesis, the process of male gamete formation from blood-circulating mature
115 male gametocytes¹⁴.

116 Identification of gametocyte-specific targets of the N-4HCS scaffold

117 To facilitate identification of potential cellular target(s) via photoaffinity labelling we first derivatised
118 **DDD01035881** to incorporate both a photo-activatable group and clickable alkyne moiety onto the
119 N-4HCS scaffold (see [Supplementary Information](#) for chemistry). Despite a number of designs,
120 the tolerance of the N-4HCS scaffold to large changes in structure was found to be limited ([Table](#)
121 [S1](#)), consistent with our previous medicinal chemistry study¹⁵. Ultimately, a strategy to incorporate
122 an alkyne handle and aryl azide moiety separately on the molecule was developed, leading to the
123 synthesis of probe **2**. Parent molecule **1** was synthesised to resemble probe **2** by retaining similar
124 structural changes to the N-4HCS scaffold without the photoactivatable and clickable moieties,
125 thus mimicking biological activity of probe **2** as a control or active competitor. Critically, parent
126 molecule **1** and probe **2** retained micromolar to nanomolar IC₅₀s in the *in vitro* male gamete
127 formation assay, respectively ([Table 1](#)).

128 Preliminary testing of probe **2** was performed to test cross-linking and ligation to azido-
129 TAMRA/biotin capture reagent (AzTB)¹⁶. Cell lysate derived from activated mature gametocytes
130 was irradiated in the presence of increasing concentrations of probe **2** or DMSO to test a probe **2**
131 concentration-dependent crosslinking of proteins. Lysate containing crosslinked proteins was then
132 ligated to AzTB capture reagent in a copper catalysed azide-alkyne cycloaddition (CuAAC).
133 Crosslinked and AzTB-ligated proteins were then enriched with streptavidin coated beads. Protein
134 labelling of enriched proteins, as determined by in-gel fluorescence (IGF), was found in the

135 presence of probe **2** and was additionally shown to be AzTB dependent, thus confirming
136 successful crosslinking and CuAAC click reactions (**Figure S1A**).

137 Target identification was subsequently carried out using a 9plex tandem mass tag (TMT)
138 methodology. Live *P. falciparum* stage V gametocyte cultures were treated with either DMSO,
139 probe **2** (10 μ M) or a combination of probe **2** and parent molecule **1** to act as a competitor (10 μ M
140 each), acquiring triplicate samples of each condition. Live treated gametocytes were irradiated at
141 254nm to crosslink probe to protein targets, then purified and lysed before ligating to AzTB in a
142 CuAAC reaction. AzTB-ligated proteins were subsequently enriched with Neutravidin agarose
143 beads before preparing peptides for TMT labelling and quantification. Peptide samples were then
144 prepared for analysis by nanoscale liquid chromatography mass spectrometry on a QExactive
145 orbitrap mass spectrometer (nLC-MS/MS). Analysis of peptides found by mass spectrometry
146 revealed 129 protein hits (for raw data see **Supporting Information**).

147 Of 129 protein hits identified, the specific probe-protein interaction profile was determined by
148 omitting any hits identified in DMSO-treated samples, excluded as non-specific binding
149 interactions. Comparing DMSO and probe **2** treated fractions, probe-specific interactions revealed
150 20 protein hits positively enriched as a specific result of probe **2** labelling and AzTB ligation, as
151 shown in **Figure 1A**. To further confirm the specificity of the interaction between probe and protein
152 hits, samples treated with probe **2** in the presence of parent molecule **1**, serving as a competitor,
153 were compared to samples treated with probe **2** alone. Compared in this way, out-competed
154 probe-specific interactions revealed 9 protein hits, depicted as negatively enriched proteins in
155 **Figure 1B**. Of these 9 hits, 6 were also positively enriched in the initial comparison of DMSO and
156 probe **2**-treated fractions (**Figure 1A**, **Table 2** and see also **Extended SI** and **Figure S1B-C**).

157 Among the 6 protein hits specific to probe **2** (**Table 2**), the protein most positively enriched when
158 comparing DMSO-treated and probe **2**-treated samples was the gametocyte-specific 16 kDa
159 *Plasmodium falciparum* vacuole membrane protein Pfs16 (PlasmoDB ID, PF3D7_0406200)¹⁷. The
160 *Plasmodium falciparum* female gametocyte-specific protein Pfg377 (PlasmoDB ID,
161 PF3D7_1250100)¹⁸ was also identified. As the N-4HCS compounds have been shown to solely
162 inhibit gametocyte viability but to exert no effect on other *Plasmodium* lifecycle stages¹⁴, Pfs16 and

163 Pfg377 were prioritised for further study. All other protein hits identified here were not specific to
164 the gametocyte stages and were therefore deemed likely to be the result of non-specific binding
165 interactions. For example, spermidine synthase, a well characterised enzyme is expressed
166 specifically during erythrocytic schizogony¹⁹ and inhibitors of the enzyme have been shown to
167 impair asexual growth^{20,21}, making it an unlikely target of the gametocyte-specific N-4HCS series.
168 Rab1B, is believed to have a potential role in ER to Golgi transport²² and shown to lie adjacent to
169 the ER in early asexual blood stages²³. Since the *Rab1B* gene is essential for asexual blood stage
170 parasite growth is it also likely the result of non-specific binding²⁴. The V-type proton ATPase has
171 been shown to function in the asexual blood stages²⁵ where it plays a critical role in maintaining the
172 parasite cytosol pH²⁶. Specific inhibitors of V-type proton ATPase have been shown to markedly
173 impact asexual growth^{27,28}, making it an unlikely target of the N-4HCS series. Much like any
174 ribosomal targeted protein, including the hit L26, it is unlikely that the transmission specific effects
175 of the N-4HCS scaffold would be mediated via inhibition of these proteins. Thus, we focused our
176 attention on the sexual-stage specificity of the N-4HCS series, prioritising hits Pfs16 and Pfg377 for
177 further validation.

178 Pfs16 is a 157-amino acid protein with two transmembrane domains and is one of the earliest
179 known markers of sexual conversion in *Plasmodium*²⁹. Importantly, with respect to validating the
180 phenotype described for the N-4HCS scaffold¹⁴, knockout of the *Pfs16* gene is known to be
181 associated with a block in microgametogenesis as is also evident with N-4HCS compound
182 treatment³⁰. Pfg377 is, in contrast, only associated with female gametocytes and would therefore
183 be less likely as a target of the N-4HCS scaffold which has been shown to specifically inhibit male
184 gamete formation. Given its phenotypic consistency with drug action, we therefore sought to further
185 validate Pfs16 as a cellular target of the compound whilst simultaneously investigating whether the
186 Pfg377 interaction is specific.

187 **Investigation of Pfs16 and Pfg377 as potential targets of the N-4HCS scaffold by PAL**

188 To validate TMT-dependent identification of Pfs16 and Pfg377 as potential N-4HCS targets, PAL
189 was repeated and analysed by IGF and immunoblot. As with the TMT identification, live mature

190 gametocytes were treated with increasing concentrations of probe **2** and irradiated with UV to
191 enable bioconjugation to cellular target(s). The probe-tagged proteins present in the resulting cell
192 lysate were biotinylated with TAMRA-containing AzTB capture reagent³¹ and pulled down with
193 streptavidin coated magnetic beads. Enriched proteins which were ligated to AzTB and thus
194 TAMRA-labelled were then analysed by IGF, performing the experiment in triplicate. A notable
195 protein band between 15 and 20kDa, likely corresponding to the 16kDa protein Pfs16,
196 demonstrated a probe **2** concentration-dependent pulldown relative to DMSO in each replicate
197 (**Figure 1C**). Densitometry revealed that the relative band intensity of the enriched protein band
198 increased with higher concentrations of probe **2** relative to a DMSO control, over each replicate
199 (**Figure 1D**). Corresponding immunoblot and densitometry was then used to analyse the specificity
200 of the pulldown to Pfs16 and Pfg377, by using increasing concentrations of probe **2**, and antibodies
201 specific to each of the proteins (see **Figure S2** for the full triplicate IGF data of protein pulldowns
202 and corresponding immunoblots). While a dose-dependent pulldown of Pfs16 was clearly observed
203 (**Figure 1E**), there was no correlation between probe **2** concentration and the amount of Pfg377
204 pulled down by the probe (**Figure 1F**), supporting our hypothesis of the latter being a non-specific
205 interaction. The dose-dependent pulldown of Pfs16, in contrast, adds further support to Pfs16
206 being the likely target of the N-4HCS series.

207 Adding further validation, pulldowns were performed on parasites treated with a combination of
208 probe **2** and parent compound **DDD01035881**, acting as a competitor. If the pulled-down protein is
209 a target of the N-4HCS scaffold, addition of a highly potent competitor should result in a decrease
210 in the amount of protein available for pull-down by the probe. A clear decrease in the protein band
211 detected at 15-20 kDa by IGF was indeed seen when comparing the pulldowns in the presence
212 and absence of parent molecule (**Figure S3**). This result confirms specific pull down of Pfs16
213 following probe **2** labelling, attributable to the N-4HCS scaffold and hence to the **DDD01035881**
214 series.

215 **Label-free validation of Pfs16 as a potential target of DDD01035881**

216 PAL is known to be vulnerable to false positive results, with clickable derivatives potentially binding
217 non-specifically to proteins besides the target of interest³². To validate the specificity of

218 **DDD01035881** engagement with proteins Pfs16 and Pfg377, the label-free Cellular Thermal Shift
219 Assay (CETSA) was used with lysate from mature gametocyte cultures and the original
220 **DDD01035881** compound. CETSA is based on the premise that proteins irreversibly aggregate
221 when thermally challenged and the modulation of a given protein when bound to a ligand can alter
222 this process, resulting in increased thermal stability³³. Using a thermal gradient, a melting curve of
223 a given protein can then be obtained to compare the protein's melting temperature (T_m) and the
224 temperature at which the protein aggregates in the presence and absence of a ligand³⁴. A positive
225 shift in a protein's T_m relative to a DMSO control would indicate protein stabilisation due to ligand
226 engagement, confirming drug binding to the protein. Melting curves and T_m can be obtained by
227 analysis of corresponding immunoblots using antibodies specific to the protein of interest,
228 permitting comparison of T_m as relative immunoblot density. We utilised in-lysate CETSA using 1%
229 Triton-X100-containing lysis buffer, which would be expected to solubilise a PVM protein target
230 such as Pfs16, prior to compound treatment and thermal challenge. The lysis conditions used
231 matched those used in the PAL target identification study.

232 Mature gametocyte cell lysate from activated stage V gametocytes was incubated with either
233 **DDD01035881** or DMSO as a control, thermally challenged and probed by immunoblot using
234 Pfs16-specific antibody¹⁷ to explore the engagement of **DDD01035881** and Pfs16 (**Figure S4**).
235 Pfs16 melt curves were obtained to compare the T_m between DMSO-treated and **DDD01035881**-
236 treated soluble gametocyte protein fractions (**Figure 2**). **DDD01035881** treatment clearly resulted
237 in a positive shift in the Pfs16 melting curve (**Figure 2A**). When compared to DMSO by
238 densitometry, the relative band-density of **DDD01035881** treated fractions were found to be
239 significantly different at 91°C (unpaired two tailed t test, $p < 0.001$). Utilising the same approach,
240 **DDD01035881** did not show significant stabilisation of Pfg377 at any temperature investigated
241 (**Figure 2B**). This aligns with the published female-specific role of the Pfg377 in
242 macrogametogenesis and lack of activity of **DDD01035881** against female gametocytes¹⁸. These
243 results strongly support a specific interaction between **DDD01035881** and Pfs16 in mature
244 activated male gametocytes, corroborating the PAL. The lack of interaction with the female-specific

245 Pfg377 suggests its detection by PAL was a false-positive, consistent with our understanding that
246 **DDD01035881** specifically targets males.

247 To further validate the positive-shift in Pfs16 T_m with **DDD01035881** treatment of activated
248 gametocyte lysate, an isothermal dose response (ITDR) format of CETSA was applied. ITDR-
249 CETSA utilises the same premise as the melt curve format, but proteins are thermally challenged
250 with a single temperature and treated with varying compound concentrations³⁵. The single
251 temperature applied in ITDR-CETSA is that at which Pfs16 is mostly aggregated in the DMSO-
252 treated fraction but is largely stabilised in the **DDD01035881** fraction (derived from the melt curve,
253 **Figure 2A**). ITDR-CETSA with **DDD01035881** was performed at 78.4°C using concentrations
254 between 1 nM and 100 µM with the results analysed by immunoblotting (**Figure 2C**). A clear
255 concentration dependent stabilisation of Pfs16 was seen, adding substantial support to Pfs16
256 being a specific interactor of the label-free **DDD01035881**.

257 **DDD01035881 specifically inhibits microgametogenesis without impacting**
258 **gametocytogenesis**

259 Pfs16 is reported to be the earliest marker of sexual conversion, with gene disruption suggesting it
260 plays a crucial role in commitment to gametocytogenesis³⁰. We therefore sought to study the effect
261 of **DDD01035881** treatment on sexual conversion and early gametocyte development. To
262 determine the stage specificity of Pfs16 binding, CETSA was performed on immature gametocyte
263 cell lysate derived from stage I-III gametocyte culture. Following an identical experimental
264 approach, stage I-III gametocyte lysates were treated with **DDD01035881** and thermally
265 challenged to quantify the stabilisation of Pfs16 and Pfg377. No positive shift or statistically
266 significant difference was found between the DMSO and **DDD01035881** treated fractions in both
267 Pfs16 (**Figure 3A**) and Pfg377 (**Figure 3B**). These findings suggest that binding of **DDD01035881**
268 is specific to Pfs16 in mature gametocytes, with no binding observed for Pfs16 in immature
269 gametocytes or Pfg377 at any stage.

270 Validation of the stage specificity of Pfs16 binding *in vitro* was determined by measuring
271 conversion rates of a transgenic *P. falciparum* line, which expresses tdTomato at the point of

272 sexual conversion (*Pf*2004/164-tdTomato³⁶) as determined by flow cytometry (**Figure S5**).

273 Conversion rates of parasites treated with 4-NHCS compounds were quantified relative to a

274 negative control. Here, gametocytes were treated with either **DDD01035881** or a DMSO under

275 multiple conditions and used to quantify i) inhibition of sexual conversion (**Figure 3C**), ii) the

276 reversibility of any inhibitory effect on conversion (**Figure 3D**) and finally, iii) effects to early

277 gametocyte development (**Figure 3E**). The respective conditions were i) prolonged compound

278 exposure from the point of induction (**Figure 3C**), ii) compound removal 24 hours post-induction

279 (**Figure 3D**) and iii) late compound treatment 24 hours after induction (**Figure 3E**, the gating

280 strategy and conversion rates of additional N-4HCS compounds can be found in **Figure S5**). We

281 found no significant reduction in conversion rates under any of the three treatment conditions,

282 suggesting that **DDD01035881** action functions specifically during microgametogenesis and not

283 sexual conversion or early gametocyte development.

284 **DDD01035881 activity window coincides with Pfs16 activity during microgametogenesis**

285 Having defined that the N-4HCS compound series likely targets Pfs16 during microgametogenesis,

286 we next sought to assess the precise cellular phenotype of the parent molecule, **DDD01035881**,

287 beginning with defining its window of action within the process of microgametogenesis. As

288 **DDD01035881** is known to inhibit microgametogenesis without requiring prior incubation with

289 gametocytes, we hypothesised the compound may continue to exert inhibitory activity beyond

290 activation of gametocytes. To narrow down an activity window for N-4HCS compounds,

291 gametocytes were activated in the absence of **DDD01035881** and subsequently treated with

292 **DDD01035881** in time increments up to the point of exflagellation. Exflagellation rates were

293 counted at 25 mins post-activation and calculated as a percentage relative to DMSO (i.e.

294 untreated) controls. As depicted in **Figure 4A**, **DDD01035881** inhibited microgametogenesis up to

295 6 min after gametocyte activation. This result is consistent with the time window when the

296 parasitophorous vacuole membrane (PVM), the membrane in which Pfs16 is found, is known to

297 function in microgametogenesis³⁷.

298 To determine whether **DDD01035881** treatment is reversible during the active window,

299 gametocytes were next treated with **DDD01035881** at the point of activation, washed to remove

300 compound and exflagellation rates measured. Reversibility of **DDD01035881** was shown to be time
301 dependent. Removal of the compound at 1 min restored exflagellation, however, inhibition was
302 retained when the compound was removed at 6 min (**Figure 4B**), the point at which **DDD01035881**
303 loses activity. Combining these observations, it can clearly be concluded that inhibition by
304 **DDD01035881** reversibly blocks microgametogenesis within a 6 min activity window post-
305 gametocyte activation. Beyond 6 min post-activation, the Pfs16-containing PVM^{17,29,38}, is lost due
306 to microgametocyte egress³⁷ and hence, loss of **DDD01035881** activity beyond the 6 min window
307 points to reversible binding to Pfs16. It is likely that upon reversibly binding to Pfs16,
308 **DDD01035881** results in the downstream inhibition of exflagellation which points to a
309 corresponding window of Pfs16 activity.

310 **DDD01035881 treatment does not impact ploidy during microgametogenesis**

311 We next sought to decipher whether **DDD01035881** treatment plays a role in DNA replication, one
312 of the key events in microgametogenesis. To determine the ploidy of gametocytes we used flow
313 cytometry analysis of a transgenic parasite, *PfDynGFP/P47mCherry*, that expresses GFP in male
314 or mCherry in female gametocytes (**Figure S6A**)³⁹. Vybrant™ DyeCycle™ Violet staining was used
315 as a measure of male gametocyte DNA content at 0 and 15 min post-activation. To measure
316 ploidy, the GFP and Vybrant™ DyeCycle™ Violet double-positive gametocyte population was
317 gated, from which discrete populations of 1n, 2n, 4n and 8n male gametocytes could then be
318 measured (**Figure S6B-D**).

319 For DMSO treated control parasites, at 0 min, gametocytes with 1n genome were the most
320 abundant, with a smaller proportion having 2n, 4n or 8n genomes. This small proportion of cells
321 with evidence of genome replication, is a probable result of premature activation or selective gene
322 amplification⁴⁰. Conversely, most gametocytes had an 8n genome at 15 min post-activation, which
323 is indicative of three successful rounds of DNA replication⁴⁰. A reduced proportion of gametocytes
324 failed to fully replicate DNA, with all 1n, 2n and 4n genomes found at different ratios. Ploidy of
325 **DDD01035881**-treated and DMSO-treated gametocytes were found to be similar at both 0 and 15
326 min post-activation, with no statistically significant difference found (**Figure 4C**). Thus, treatment
327 with **DDD01035881** does not lead to a defect to in replication during microgametogenesis. Thus, if

328 **DDD01035881** targets Pfs16, by extension this suggest that Pfs16 does not function in or signal
329 upstream of DNA replication (**Figure 4C**).

330 **DDD01035881 treatment disrupts cytoskeletal, nuclear and food vacuole structure**

331 Having defined that **DDD01035881** activity is specific to microgametogenesis without impacting
332 gametocytogenesis, we next sought to define the compound phenotype during
333 microgametogenesis. Perturbances to microgametogenesis under **DDD01035881** treatment were
334 analysed by either immunofluorescence (IF) microscopy or electron microscopy, using DMSO-
335 treated gametocytes as a control (**Figure S7**).

336 First, IF analysis was used to determine the effects of compound treatment on cytoskeletal
337 rearrangement, host erythrocyte egress and DNA replication. Gametocytes were first activated in
338 the absence of drug and then treated with **DDD01035881** at various timepoints relative to
339 activation, before being fixed and stained for analysis. As shown in **Figure 4D**, **DDD01035881**
340 treatment resulted in a perturbation to microgametogenesis compared to DMSO-treated
341 gametocytes. The morphological phenotype found under **DDD01035881** treatment was found to be
342 treatment-time dependent with distinct phenotypes observed depending on time of treatment
343 relative to activation.

344 **DDD01035881** treatment at 0-0.5 min post-activation blocked exflagellation and the cytoskeletal
345 rearrangement of parasites, with gametocytes failing to form mitotic spindles or axonemes.
346 Gametocytes succeeded in rounding up, but the egress phenotype was mixed, with some
347 parasites failing and some succeeding to egress from the host erythrocyte (**Figure 4D**). From 1-2
348 min, exflagellation failed and the parasite cytoskeleton, depicted as labelled alpha tubulin, adopted
349 a figure-of-eight morphology. The mixed egress phenotype was retained, with erythrocyte vesicles
350 remaining close to the parasite as expected in microgametogenesis³⁷; those failing to egress also
351 demonstrated some erythrocyte vesiculation, although to a lesser extent. DNA staining suggested
352 replication was successful, with DNA either localising to one or both sides of the figure-of-eight.
353 Similarly, treatment from 4-5 min resulted in a cytoskeletal figure-of-eight morphology, but egress
354 and erythrocyte vesiculation was successful. However, a truncated flagellar formed from the larger

355 side of the figure-of-eight with tubulin staining markedly more diffuse on the opposing end of the
356 parasite. From 6-25 min, exflagellation appeared to match that of the DMSO control (**Figure 4D**),
357 although the onwards viability of gametes was not determined. Should Pfs16 be the target of
358 **DDD01035881**, this points to a potential function of the protein upstream of cytoskeletal
359 rearrangements that underpin microgamete development.

360 Electron microscopy was used to bring ultrastructural insight into the **DDD01035881** phenotype.
361 Gametocytes were treated with either compound or DMSO prior to activation and fixed at 25 min
362 post-activation. **Figure 4E** showed an example of a DMSO-treated control gametocytes preparing
363 for exflagellation, forming the characteristic 9+2 organisation of microtubules which emerge as
364 gametes (**Figure 4H**). In contrast, gametocytes treated with **DDD01035881** prior to activation
365 demonstrated a disruption to the structural integrity of the nucleus and food vacuole, with multiple
366 haemozoin-containing vesicles dispersed across the cytosol of the parasite (**Figure 4F**). This
367 finding was consistent with the phenotype of previously described lines with targeted gene
368 disruption of the *Pfs16* gene³⁰. The mixed egress phenotype was visualised with gametocytes
369 lacking (**Figure 4F**) and retaining the 4-layer membrane (**Figure 4G**). Again, if **DDD01035881**
370 treatment results in inhibition of microgametogenesis due to Pfs16 binding, the compound could
371 serve as a tool for understanding Pfs16 function, which is yet to be fully elucidated.

372 Of note, the phenotypes seen with **DDD01035881** treatment by IF were markedly different to
373 inhibition of microgametogenesis when targeting calcium-dependent protein kinase 4 (CDPK4)
374 (using inhibitor 1294⁴¹), cyclic-GMP dependent protein kinase (PKG) (using the inhibitor ML10⁴²) or
375 canonical inhibitors of microtubules (Colchicine) or actin microfilaments (Cytochalasin B) (**Figure**
376 **S8**). The specific activity windows of 1294 and ML10, 0-20 sec and 0-8 min, respectively, were
377 also markedly different from that of **DDD01035881**, suggesting that compound activity has a
378 discrete function to that of these known regulators of microgametogenesis.

379 **DDD01035881 treated parasites demonstrate disruption of parasitophorous vacuole and**
380 **Pfs16 release**

381 Finally, having defined when the compound series is active, we next sought to correlate
382 **DDD01035881** action with the cellular distribution and effects of Pfs16 during microgametogenesis
383 ³⁰. Pfs16 is known to be localised to the PVM^{17,29,38}, which vesiculates and disintegrates prior to the
384 host erythrocyte in an inside-out mechanism of egress during microgametogenesis³⁷. Following
385 egress, Pfs16 has been detected in both so-called “Garnham” bodies and multi-laminated whorls
386 formed from the PVM after rupture³⁸. By IF labelling of Pfs16, we could show that Pfs16
387 surrounded microgametocytes at 0 min before either capping or forming a pore at a single side of
388 the activated gametocyte in preparation for egress at around 5.5 min (**Figure 5A**). Upon egress
389 from the host erythrocyte, Pfs16 localised to vesicles which are expelled from the single pore or
390 cap at 6.5 min. Minimal remnants of Pfs16 were seen to remain attached to the parasite from 8.5
391 min, with no Pfs16 detected on microgametes at 20 min (**Figure 5A**).

392 At egress, **DDD01035881** treatment was found to disrupt Pfs16 localisation with two distinct
393 phenotypes (**Figure 5B**). In the first, gametocytes failed to egress from the host erythrocyte with
394 Pfs16 retaining expression at the PVM that, as well as the erythrocyte, does not disintegrate or
395 vesiculate. In the second, successful but aberrant erythrocyte egress was detected, as Pfs16
396 capped to a single end of the parasite but failed to vesiculate and erupt from a pore. With the latter,
397 minimal remnants of Pfs16 were detected at 8.5 min, with no detectable WGA staining. These
398 results demonstrate **DDD01035881** inhibition often disrupts the expulsion of the PVM and
399 associated Pfs16 during microgametogenesis. The combined weight of experimental data
400 therefore not only points to Pfs16 being the target of the N-4HCS scaffold but corroborates Pfs16's
401 key role in PVM degradation being a critical step in microgametogenesis.

402 **DISCUSSION**

403 As resistance inevitably threatens the long-term success of artemisinin and its derivatives in
404 treating malaria disease, there is an urgent need for new antimalarials with novel chemotypes and
405 modes of action⁴³. Here, we have validated the cellular effects of a potent transmission blocking
406 compound series based on an N-4HCS scaffold and identified the *Plasmodium falciparum* 16 kDa
407 protein, Pfs16, as a highly promising cellular target. The hit compound series was first identified in
408 a cell-based high throughput screen¹⁴, with hits further optimised by medicinal chemistry¹⁵. The N-
409 4HCS activity profile fits with the Medicines for Malaria Venture target candidate profile 5 (TCP5)
410 that covers transmission blocking interventions⁴³. With identification of its target, and its low
411 cytotoxicity, the N-4HCS scaffold is clearly poised for development as a combination, transmission
412 blocking therapeutic.

413 Based on detailed phenotypic analysis, the N-4HCS series specifically results in the potent
414 inhibition of microgametogenesis, though without impacting sexual conversion or early gametocyte
415 development. However, the phenotypic effect of the compounds is clear and rapid, traversing the
416 erythrocyte membrane and having action within the first 0-6 min post-activation of parasites. The
417 activity window supports evidence that the Pfs16 protein function is vital to microgametogenesis in
418 its earliest stages, during which the PVM remains associated with the parasite. Beyond PVM
419 expulsion from 6 min, compound effects halt, suggesting that Pfs16 is no longer essential beyond
420 this point. This fits broadly with gene knockout studies for *Pfs16*³⁰.

421 One inconsistency that was noted is that **DDD01035881**-treated parasites did not show any defect
422 in gametocyte commitment, noted as a *Pfs16* knockout phenotype. This may be due to the target
423 site of the Pfs16 protein. A previous study on protein trafficking across the PV to the PVM in *P.*
424 *falciparum* used parasites transformed with different Pfs16-GFP constructs to determine the amino
425 acid sequences required for PVM targeting and retention⁴⁴. Interestingly, the study suggested the
426 region for PVM targeting and retention differs from the region required for capping during
427 gametogenesis, supporting a dual role for the protein. PVM targeting and retention was shown to
428 be sufficient with inclusion of the 53 C-terminal AA of Pfs16, containing a motif conserved in other
429 known PVM proteins, and N-terminal secretory signal sequence. The specific signal for PVM

430 targeting was localised to 42 AAs comprising the transmembrane domain (22 AA) and part of the
431 C-terminal tail (20 of the 31 AA). The protein membrane interaction was found to be stabilised with
432 11 C-terminal AA, which when removed reduced the level of retention but did not affect PVM
433 targeting. In contrast, amino acids between the N-terminal secretory signal sequence and
434 transmembrane domain were found to be crucial for capping involved in egress during
435 gametogenesis, though not required for PVM targeting⁴⁴. This difference in function of the different
436 regions of the Pfs16 protein may clarify why the N-4HCS series specifically targets gametogenesis
437 but fails to inhibit commitment to gametocyte formation, despite the protein being present in both
438 stages. Thus, the compound series may potentially bind the region involved in capping; a region
439 suggested to be located within the PV in association with the gametocyte surface. In contrast, the
440 region involved in membrane retention which likely falls on the erythrocyte side of the PVM, a
441 region also shown to be conserved in other PVM proteins, is unlikely to be the target and therefore
442 might explain the specific phenotype of N-4HCS treatment. Further structural investigation of the
443 specific binding of **DDD01035881** to the Pfs16 protein is clearly required to test this hypothesis.

444 Targeting sexual conversion with antimalarials represents several challenges. Exploiting early
445 commitment or development in a clinical setting is particularly challenging since these parasites
446 develop cryptically in the mammalian host¹⁰. However, targeting the mature gametocytes to
447 prevent onwards transmission provides several avenues for drug development⁴³. This is where the
448 microgametogenesis targeted-activity of the N-4HCS series may be particularly valuable. The
449 immediate and potent activity of **DDD01035881**, for example, upon activation of gametogenesis
450 (and proven activity in a murine *in vivo* model in this context¹⁴) gives confidence about the ability of
451 this series to halt parasite development in the mosquito vector. However, for effective inhibition of
452 gametogenesis to occur following a mosquito feed, the compound would need to last long enough
453 in circulation to be taken up by a feeding mosquito. This likely represents the key challenge for this
454 class of molecule. Approaches that may work in this context would be further medicinal chemistry
455 to increase the longevity/bioavailability of this scaffold in the blood stream (current evidence
456 suggests it may only last an hour or so¹⁴). Alternatively, other approaches to maximise longevity
457 might include formulation for slow release, such as via engineering nanoparticles or other

458 substrates, which facilitate slow release in the blood stream⁴⁵. Recent work has explored
459 impregnation of bed nets or other bait sources with antimalarials to target transmission directing
460 drug uptake to the mosquito not the human host^{46,47}. Such an approach may work well with the N-
461 4HCS compound series.

462 A constant challenge with mode of action identification in *Plasmodium* sexual stages is that these
463 stages of the lifecycle do not replicate. This means that *in vitro* evolution and whole genome
464 analysis (IVIEWGA), a method in which parasites are continually exposed to antimalarial
465 compounds of interest to yield resistance before determining the genetic basis of resistance⁴⁸, will
466 not work⁴⁸. Thus, whilst this chemogenetic approach has been hugely valuable in mapping the
467 druggable genome it remains unattainable for studying targets of compounds which specifically
468 inhibit viability of the sexual stages. This demonstrates the power of CETSA, especially with
469 advancement of protocols specifically for *P. falciparum* drug-target identification⁴⁹. A recent proof-
470 of-concept study used CETSA coupled to mass spectrometry, with both a whole cell and cell lysate
471 approach, to validate targets of pyrimethamine and E64d. Having proven CETSA to be efficacious
472 and robust, the study went on to define to MoA of quinolone drugs, quinine and mefloquine⁵⁰.
473 Although the majority of CETSA studies have been applied to soluble proteins, ligand stabilisation
474 of detergent solubilised membrane proteins has also been successfully achieved^{51,52}. An in-depth
475 study on multipass transmembrane proteins utilised live cell CETSA with a range of concentrations
476 of varying detergents, which were added after the compound treatment and thermal challenge of
477 cells⁵². Here, we have demonstrated the power of PAL combined with CETSA in the identification
478 and validation of a PVM cellular target from cellular phenotypic screen-derived hits.

479 In summary, we have identified Pfs16, described as the earliest marker of sexual conversion, as a
480 very strong candidate for the cellular target of the N-4HCS transmission blocking compound
481 scaffold. Further investment in both the compound but also the protein target itself is now clearly
482 warranted, with the structure of the protein and subsequent attempts at co-crystallisation being a
483 key priority. With further development in the chemistry of transmission blocking drugs and the
484 exploration of avenues to either co-formulate with treatment drugs or deliver via alternative vector
485 targeting approaches, transmission blocking drugs should strongly be considered as important

486 components of future antimalarial combination therapies. With the SARS-CoV-2 pandemic
487 threatening to take resources away from malaria and the looming possibilities of a resurgence of
488 malaria incidence in the developing world, new strategies to break the cycle of infection are more
489 important than ever.

490

491 **REFERENCES AND NOTES**

- 492 1. WHO. World Malaria Report. (Geneva, 2019).
- 493 2. Prudencio, M., Rodriguez, A. & Mota, M.M. The silent path to thousands of merozoites: the
494 Plasmodium liver stage. *Nat Rev Microbiol* **4**, 849-56 (2006).
- 495 3. Wells, T.N., Hooft van Huijsduijnen, R. & Van Voorhis, W.C. Malaria medicines: a glass half full? *Nat*
496 *Rev Drug Discov* **14**, 424-42 (2015).
- 497 4. Sinden, R.E. Developing transmission-blocking strategies for malaria control. *PLoS Pathog* **13**,
498 e1006336 (2017).
- 499 5. Graumans, W., Jacobs, E., Bousema, T. & Sinnis, P. When Is a Plasmodium-Infected Mosquito an
500 Infectious Mosquito? *Trends Parasitol* **36**, 705-716 (2020).
- 501 6. Blagborough, A.M. et al. Transmission-blocking interventions eliminate malaria from laboratory
502 populations. *Nat Commun* **4**, 1812 (2013).
- 503 7. Yahiya, S., Rueda-Zubiaurre, A., Delves, M.J., Fuchter, M.J. & Baum, J. The antimalarial screening
504 landscape-looking beyond the asexual blood stage. *Curr Opin Chem Biol* **50**, 1-9 (2019).
- 505 8. Birkholtz, L.M., Coetzer, T.L., Mancama, D., Leroy, D. & Alano, P. Discovering New Transmission-
506 Blocking Antimalarial Compounds: Challenges and Opportunities. *Trends Parasitol* **32**, 669-681
507 (2016).
- 508 9. Ashley, E.A., Recht, J. & White, N.J. Primaquine: the risks and the benefits. *Malar J* **13**, 418 (2014).
- 509 10. Ngotho, P. et al. Revisiting gametocyte biology in malaria parasites. *FEMS Microbiol Rev* **43**, 401-
510 414 (2019).
- 511 11. Sinden, R.E., Canning, E.U., Bray, R.S. & Smalley, M.E. Gametocyte and gamete development in
512 Plasmodium falciparum. *Proc R Soc Lond B Biol Sci* **201**, 375-99 (1978).
- 513 12. Sinden, R.E. Gametocytogenesis of Plasmodium falciparum in vitro: an electron microscopic study.
514 *Parasitology* **84**, 1-11 (1982).
- 515 13. Hughes, J.P., Rees, S., Kalindjian, S.B. & Philpott, K.L. Principles of early drug discovery. *Br J*
516 *Pharmacol* **162**, 1239-49 (2011).
- 517 14. Delves, M.J. et al. A high throughput screen for next-generation leads targeting malaria parasite
518 transmission. *Nat Commun* **9**, 3805 (2018).
- 519 15. Rueda-Zubiaurre, A. et al. Structure-activity relationship studies of a novel class of transmission
520 blocking antimalarials targeting male gametes. *J Med Chem* (2019).
- 521 16. Wright, M.H. et al. Global analysis of protein N-myristoylation and exploration of N-
522 myristoyltransferase as a drug target in the neglected human pathogen Leishmania donovani.
523 *Chem Biol* **22**, 342-54 (2015).
- 524 17. Bruce, M.C., Carter, R.N., Nakamura, K., Aikawa, M. & Carter, R. Cellular location and temporal
525 expression of the Plasmodium falciparum sexual stage antigen Pfs16. *Mol Biochem Parasitol* **65**, 11-
526 22 (1994).
- 527 18. de Koning-Ward, T.F. et al. The role of osmiophilic bodies and Pfg377 expression in female
528 gametocyte emergence and mosquito infectivity in the human malaria parasite Plasmodium
529 falciparum. *Mol Microbiol* **67**, 278-90 (2008).
- 530 19. Haider, N. et al. The spermidine synthase of the malaria parasite Plasmodium falciparum: molecular
531 and biochemical characterisation of the polyamine synthesis enzyme. *Mol Biochem Parasitol* **142**,
532 224-36 (2005).
- 533 20. Sprenger, J. et al. Three-dimensional structures of Plasmodium falciparum spermidine synthase
534 with bound inhibitors suggest new strategies for drug design. *Acta Crystallogr D Biol Crystallogr* **71**,
535 484-93 (2015).
- 536 21. Dufe, V.T. et al. Crystal structure of Plasmodium falciparum spermidine synthase in complex with
537 the substrate decarboxylated S-adenosylmethionine and the potent inhibitors 4MCHA and
538 AdoDATO. *J Mol Biol* **373**, 167-77 (2007).
- 539 22. Quevillon, E. et al. The Plasmodium falciparum family of Rab GTPases. *Gene* **306**, 13-25 (2003).
- 540 23. Taku, I. et al. Rab5b-Associated Arf1 GTPase Regulates Export of N-Myristoylated Adenylate Kinase
541 2 From the Endoplasmic Reticulum in Plasmodium falciparum. *Front Cell Infect Microbiol* **10**,
542 610200 (2020).

- 543 24. Zhang, M. et al. Uncovering the essential genes of the human malaria parasite *Plasmodium*
544 *falciparum* by saturation mutagenesis. *Science* **360**(2018).
- 545 25. Hayashi, M. et al. Vacuolar H(+)-ATPase localized in plasma membranes of malaria parasite cells,
546 *Plasmodium falciparum*, is involved in regional acidification of parasitized erythrocytes. *J Biol Chem*
547 **275**, 34353-8 (2000).
- 548 26. van Schalkwyk, D.A. et al. Inhibition of *Plasmodium falciparum* pH regulation by small molecule
549 indole derivatives results in rapid parasite death. *Biochem Pharmacol* **79**, 1291-9 (2010).
- 550 27. Auparakkitanon, S. & Wilairat, P. Antimalarial activity of concanamycin A alone and in combination
551 with pyronaridine. *Southeast Asian J Trop Med Public Health* **37**, 619-21 (2006).
- 552 28. Bray, P.G., Howells, R.E. & Ward, S.A. Vacuolar acidification and chloroquine sensitivity in
553 *Plasmodium falciparum*. *Biochem Pharmacol* **43**, 1219-27 (1992).
- 554 29. Lanfrancotti, A., Bertuccini, L., Silvestrini, F. & Alano, P. *Plasmodium falciparum*: mRNA co-
555 expression and protein co-localisation of two gene products upregulated in early gametocytes. *Exp*
556 *Parasitol* **116**, 497-503 (2007).
- 557 30. Kongkasuriyachai, D., Fujioka, H. & Kumar, N. Functional analysis of *Plasmodium falciparum*
558 parasitophorous vacuole membrane protein (Pfs16) during gametocytogenesis and gametogenesis
559 by targeted gene disruption. *Mol Biochem Parasitol* **133**, 275-85 (2004).
- 560 31. Broncel, M. et al. Multifunctional reagents for quantitative proteome-wide analysis of protein
561 modification in human cells and dynamic profiling of protein lipidation during vertebrate
562 development. *Angew Chem Int Ed Engl* **54**, 5948-51 (2015).
- 563 32. Smith, E. & Collins, I. Photoaffinity labeling in target- and binding-site identification. *Future Med*
564 *Chem* **7**, 159-83 (2015).
- 565 33. Martinez Molina, D. et al. Monitoring drug target engagement in cells and tissues using the cellular
566 thermal shift assay. *Science* **341**, 84-7 (2013).
- 567 34. Jafari, R. et al. The cellular thermal shift assay for evaluating drug target interactions in cells. *Nat*
568 *Protoc* **9**, 2100-22 (2014).
- 569 35. Black, R.E. et al. Global, regional, and national causes of child mortality in 2008: a systematic
570 analysis. *Lancet* (2010).
- 571 36. Brancucci, N.M., Goldowitz, I., Buchholz, K., Werling, K. & Marti, M. An assay to probe *Plasmodium*
572 *falciparum* growth, transmission stage formation and early gametocyte development. *Nat Protoc*
573 **10**, 1131-42 (2015).
- 574 37. Andreadaki, M. et al. Sequential Membrane Rupture and Vesiculation during *Plasmodium berghei*
575 Gametocyte Egress from the Red Blood Cell. *Sci Rep* **8**, 3543 (2018).
- 576 38. Baker, D.A., Daramola, O., McCrossan, M.V., Harmer, J. & Targett, G.A. Subcellular localization of
577 Pfs16, a *Plasmodium falciparum* gametocyte antigen. *Parasitology* **108** (Pt 2), 129-37 (1994).
- 578 39. Lasonder, E. et al. Integrated transcriptomic and proteomic analyses of *P. falciparum* gametocytes:
579 molecular insight into sex-specific processes and translational repression. *Nucleic Acids Res* **44**,
580 6087-101 (2016).
- 581 40. Janse, C.J. et al. DNA synthesis in gametocytes of *Plasmodium falciparum*. *Parasitology* **96** (Pt 1), 1-
582 7 (1988).
- 583 41. Ojo, K.K. et al. A specific inhibitor of PfCDPK4 blocks malaria transmission: chemical-genetic
584 validation. *J Infect Dis* **209**, 275-84 (2014).
- 585 42. Baker, D.A. et al. A potent series targeting the malarial cGMP-dependent protein kinase clears
586 infection and blocks transmission. *Nat Commun* **8**, 430 (2017).
- 587 43. Burrows, J.N. et al. New developments in anti-malarial target candidate and product profiles. *Malar*
588 *J* **16**, 26 (2017).
- 589 44. Eksi, S. & Williamson, K.C. Protein targeting to the parasitophorous vacuole membrane of
590 *Plasmodium falciparum*. *Eukaryot Cell* **10**, 744-52 (2011).
- 591 45. Kamaly, N., Yameen, B., Wu, J. & Farokhzad, O.C. Degradable Controlled-Release Polymers and
592 Polymeric Nanoparticles: Mechanisms of Controlling Drug Release. *Chem Rev* **116**, 2602-63 (2016).
- 593 46. Fiorenzano, J.M., Koehler, P.G. & Xue, R.D. Attractive Toxic Sugar Bait (ATSB) For Control of
594 Mosquitoes and Its Impact on Non-Target Organisms: A Review. *Int J Environ Res Public Health*
595 **14**(2017).

- 596 47. Paton, D.G. et al. Exposing Anopheles mosquitoes to antimalarials blocks Plasmodium parasite
597 transmission. *Nature* **567**, 239-243 (2019).
- 598 48. Luth, M.R., Gupta, P., Otilie, S. & Winzeler, E.A. Using in Vitro Evolution and Whole Genome
599 Analysis To Discover Next Generation Targets for Antimalarial Drug Discovery. *ACS Infect Dis* **4**, 301-
600 314 (2018).
- 601 49. Dziekan, J.M. et al. Cellular thermal shift assay for the identification of drug-target interactions in
602 the Plasmodium falciparum proteome. *Nat Protoc* (2020).
- 603 50. Dziekan, J.M. et al. Identifying purine nucleoside phosphorylase as the target of quinine using
604 cellular thermal shift assay. *Sci Transl Med* **11**(2019).
- 605 51. Ashok, Y., Nanekar, R. & Jaakola, V.P. Defining thermostability of membrane proteins by western
606 blotting. *Protein Eng Des Sel* **28**, 539-42 (2015).
- 607 52. Kawatkar, A. et al. CETSA beyond Soluble Targets: a Broad Application to Multipass Transmembrane
608 Proteins. *ACS Chem Biol* **14**, 1913-1920 (2019).
- 609 53. UniProt, C. UniProt: a worldwide hub of protein knowledge. *Nucleic Acids Res* **47**, D506-D515
610 (2019).
- 611 54. Delves, M.J. et al. Routine in vitro culture of P. falciparum gametocytes to evaluate novel
612 transmission-blocking interventions. *Nat Protoc* **11**, 1668-80 (2016).
- 613 55. Cox, J. & Mann, M. MaxQuant enables high peptide identification rates, individualized p.p.b.-range
614 mass accuracies and proteome-wide protein quantification. *Nat Biotechnol* **26**, 1367-72 (2008).
- 615 56. UniProt: a worldwide hub of protein knowledge. *Nucleic Acids Res* **47**, D506-d515 (2019).
- 616 57. Kulak, N.A., Pichler, G., Paron, I., Nagaraj, N. & Mann, M. Minimal, encapsulated proteomic-sample
617 processing applied to copy-number estimation in eukaryotic cells. *Nat Methods* **11**, 319-24 (2014).
- 618 58. Moelans, I.I.M.D. *Pfs16, a potential vaccine candidate against the human malaria parasite*
619 *Plasmodium falciparum*, ([Sl: sn], 1995).
- 620 59. Ishino, T. et al. Observation of morphological changes of female osmiophilic bodies prior to
621 Plasmodium gametocyte egress from erythrocytes. *Mol Biochem Parasitol* **236**, 111261 (2020).
- 622 60. Fang, H. et al. Multiple short windows of calcium-dependent protein kinase 4 activity coordinate
623 distinct cell cycle events during Plasmodium gametogenesis. *Elife* **6**(2017).
- 624 61. Ayuso, M.I., Garcia-Bonilla, L., Martin, M.E. & Salinas, M. Assessment of protein expression levels
625 after transient global cerebral ischemia using an antibody microarray analysis. *Neurochem Res* **35**,
626 1239-47 (2010).

627

628 ACKNOWLEDGEMENTS

629 We thank Kathrin Witmer, Alisje Churchyard, Irene Garcia-Barbazan, Oriol Llorà-Batlle, Farah
630 Dahalan, Eliana Real and David Grimson, for assisting with parasite culture and for sharing expert
631 transmission blocking advice. Additional thanks to other members of the Baum lab, Fuchter group
632 and Tate lab for assistance with this study. We thank George Ashdown (Baum lab) for assistance
633 in design of imaging experiments, Jane Srivastava and Jessica E Rowley of the Imperial College
634 London flow cytometry facility for assistance in all flow cytometry-based experiments and Ryan
635 Howard and Henry Benns for assisting in the design of photoaffinity labelling experiments. We
636 thank Beatriz Urones Ruano, Ollala Sanz and Sonja Ghidelli-Disse at GSK and Cellzome for
637 helpful discussions and experimental support. We also acknowledge Mathieu Brochet and

638 colleagues for providing assistance in the design of the flow cytometry-based assay for
639 measurements. Finally, we gratefully acknowledge the key role of the Dundee Drug Discovery unit
640 in putting together the original Global Health Chemical Diversity Library (GHCDL) library and
641 generous collaborators who kindly donated parasite lines, additional drugs and antibody reagents
642 critical for completion of this study (Baker, Ishino, Lasonder, Marti, Sauerwein and Van Voorhis
643 labs).

644 **AUTHOR CONTRIBUTIONS**

645 S.Y., C.N.S, U.S., O.J.F., A.R.Z, S.H., G.V.B., S.J., S.H., M.J.D, E.W.T., A.B., M.J.F and J.B.
646 designed experiments. S.Y., C.N.S, U.S., O.J.F., A.R.Z, S.H., G.V.B. and S.J. performed
647 experiments. S.Y., C.N.S. and J.B. wrote the manuscript. All authors contributed to manuscript
648 preparation.

649 **COMPETING INTERESTS**

650 The authors declare no competing interests.

651 **DATA AVAILABILITY**

652 Raw proteomics data is attached in the extended supplementary information. Raw files analysed in
653 MaxQuant (version 1.6.1.0) were searched against the curated Uniprot *P.falciparum* NF54
654 proteome⁵³ using the built-in Andromeda search engine.

655 The PlasmoDB database (<https://plasmodb.org/>) was used to analyse protein expression.

656 **FUNDING**

657 S.Y. is supported by a Ph.D. studentship from an EPSRC Doctoral Training Partnership award
658 (Grant EP/R512540/1) to Imperial College London. This work was funded by grants from the Bill &
659 Melinda Gates Foundation (OPP1181199, JB), Wellcome (Investigator Award to JB,
660 100993/Z/13/Z) and the Medicines for Malaria Venture (RD-08-2800, JB). Microscopy work was
661 supported through the Facility for Imaging by Light Microscopy (FILM) at Imperial College London,
662 supported by previous funding from Wellcome (Grant 104931/Z/14/Z) and the Biotechnology and
663 Biological Sciences Research Council (BBSRC), UK (Grant BB/L015129/1). C.N.S was supported

664 by the Institute for Chemical Biology, EPSRC Centre for Doctoral Training (Imperial College
665 London), EPSRC Grant EP/L015498/1. M. J. F. would like to thank the EPSRC for an Established
666 Career Fellowship (EP/R00188X/1). A.B. is supported by a Sir Henry Dale Fellowship jointly
667 funded by the Wellcome Trust and the Royal Society (213435/Z/18/Z).

668

669 MATERIALS AND METHODS

670 **In vitro culture of *P. falciparum* NF54 asexual blood stages and gametocytes**

671 *P. falciparum* NF54 strain (sourced from MR4 <https://www.beiresources.org/About/MR4.aspx>),
672 *PfDynGFP/P47mCherry* (kindly gifted by Edwin Lasonder, Richard Bartfai and colleagues³⁹) and
673 *Pf2004/164-tdTom* parasites (kindly gifted by Nicolas Brancucci and Matthias Marti³⁶) were
674 cultured for asexual and sexual stage growth as previously described⁵⁴. In brief, asexual blood
675 stage cultures were maintained at 0.75-5% parasitaemia and 4% haematocrit using O+ or A+
676 human erythrocytes (NHS National Blood Service) supplemented with 30 units/ml heparin (Sigma-
677 Aldrich). Culture medium was prepared from RPMI-1640 with 25mM HEPES (Life Technologies),
678 supplemented with 50 µg/ml hypoxanthine (Sigma), 2 g/l sodium bicarbonate and 10% A+ human
679 serum (Interstate Blood-Bank). CM was changed daily, and cultures were maintained at 37°C
680 under 3% O₂/5% CO₂/92% N₂ gas (BOC Special Gases). For *Pf2004/164-tdTom* parasites,
681 asexual parasites and gametocytes were cultured as described, but maintained at 5% haematocrit
682 in media supplemented with 4nM WR 99210.

683 Gametocytes were induced from asexual blood stage cultures at 3% parasitaemia and 4%
684 haematocrit. Gametocytes were grown in RPMI-1640 with 25mM HEPES supplemented with 2
685 mg/ml D-glucose, 150 µg/ml L-glutamine, 2.78 mg/ml sodium bicarbonate, 50 µg/ml hypoxanthine,
686 5% A+ human serum and 5% AlbuMAX II (Life Technologies). Gametocyte media was changed
687 daily without the addition of fresh erythrocytes for 14 days following induction, at which point stage
688 V gametocytes were most abundant. The functional viability of gametocytes was determined at day
689 14 post-induction by measuring percentage exflagellation relative to total erythrocyte density.
690 Cultures were activated with ookinete medium (culture medium prepared as above supplemented
691 with 100µM xanthurenic acid, lacking serum or AlbuMAX II) and exflagellation events were counted
692 with a haemocytometer (VWR) using a Nikon Leica DC500 microscope.

693 **Compounds**

694 **DDD01035881** and **DDD01028076** were purchased from Life Chemicals Inc. and maintained at
695 10mM in DMSO (Honeywell). **DDD01028076** was also synthesised by ARZ in house¹⁵.

696 For full methods on the synthesis of clickable derivatives of the N-4HCS series, see
697 [Supplementary Materials and Methods](#). ML10 was kindly donated by the Baker lab⁴² whilst BKI-
698 1294 was kindly donated by the Van Voorhis lab⁴¹. Colchicine and Cytochalasin B were
699 commercially sourced. All compounds were made up to 10mM stock solutions in DMSO
700 (Honeywell) and stored at -20°C.

701 **Activated gametocyte lysate preparation**

702 Stage V *P. falciparum* NF54 gametocytes were purified by differential sedimentation using
703 NycoPrep™ 1.077 to remove the asexual parasite reservoir. Purified gametocytes were treated
704 with ookinete medium to activate gametogenesis before halting the process at 2 minutes post-
705 activation at 4°C with 0.01% saponin, used to lyse erythrocytes. 5 saponin lysis steps were
706 repeated at 4°C and parasites were washed in PBS before snap freezing in liquid nitrogen and
707 storing at -80°C. Pellets were used in lysate labelling assays and CETSA.

708 **TARGET IDENTIFICATION**

709 **Lysate Labelling Assays for In-Gel Fluorescence**

710 **Probe 2 Treatment of Cell Lysate**

711 For in-gel fluorescence detection of probe **2**-treated lysate ([Figure S1A](#)), 120ml of untreated *P.*
712 *falciparum* NF54 stage V gametocyte culture was purified using NycoPrep™ 1.077 and saponin
713 lysis as above. The resulting cell pellet was lysed by gentle agitation in 1.2 ml lysis buffer (1%
714 Triton-X100, 10 mM Tris, 150 mM NaCl, 1 x Complete EDTA-free protease inhibitor (Roche
715 Diagnostics)) for 30 min at 4°C. Protein concentration was determined using the BioRad DC
716 Protein Assay, performed according to the manufacturer's instructions. Absorbance was measured
717 at 750 nm and bovine serum albumin was used as a protein standard. 96-well plates were used to
718 measure absorbance using a SpectraMax M2e Microplate Reader (Molecular Devices). Lysates
719 were made up to 1 mg/mL in lysis buffer, transferred to microcentrifuge tubes and centrifuged
720 (17,000 x *g*, 10 min, 4°C) to remove insoluble cellular debris. Protein was divided across six
721 aliquots of 200 µl before treatment with probe **2** or DMSO, under conditions stated in [Table S2](#).
722 Samples were incubated at 4°C for 30 min and irradiated by UV at 254 nm for 5 min.

723 **Copper catalysed azide-alkyne cycloaddition (CuAAC) and protein precipitation**

724 A click reaction master mix was prepared by combining the following reagents in order:

- 725 1. AzTB capture reagent¹⁶ (1 vol of 10 mM DMSO stock; 0.1 mM final concentration)
- 726 2. CuSO₄ (2 vol of 50 mM H₂O stock; 1 mM final concentration)
- 727 3. TCEP (2 vol of 50 mM H₂O; 1 mM final concentration)
- 728 4. TBTA (1 vol of 10 mM DMSO stock; 0.1 mM final concentration).

729 6 µl of this master mix was added per 100 µl protein sample, vortexed and incubated with
730 moderate shaking for 1 hour at RT. For negative click control samples, H₂O was added in place of
731 the CuSO₄ catalyst. The reaction was quenched by addition of 5mM EDTA (from a 500 mM stock
732 in H₂O). Proteins were precipitated by addition of MeOH (4 vol), chloroform (1 vol) and H₂O (3 vol)
733 for nLC-MS/MS, or MeOH (2 vol), chloroform (0.5 vol) and H₂O (1 vol) for gel-based analysis.
734 Precipitated proteins were centrifuged at 17,000 x *g* for 2 min at 4°C. The protein pellet was
735 isolated by removal of the chloroform and MeOH/H₂O layers and washed with MeOH (4 vol).
736 Protein was then sonicated and transferred to -80°C storage for a minimum of 20 minutes.
737 Samples were centrifuged (17,000 x *g*, 5 min), MeOH was removed and the resulting protein was
738 air dried for 5 min at RT. The protein pellet was resolubilised in 2% SDS and sonicated until fully
739 dissolved before dilution to 0.2% SDS in 1 x PBS solution.

740 **Pull-down with Dynabeads (Streptavidin MyOne)**

741 Probe **2**-treated and AzTB-labelled cell lysate samples to be analysed by in-gel fluorescence (IGF)
742 were incubated with magnetic Dynabeads (Streptavidin MyOne). Beads were prewashed with 3
743 vol. of 0.2% SDS, rotary mixing for 3 min at RT. Samples were added to beads and moderately
744 shaken for 2 hours at RT. Supernatant was removed, retaining an aliquot for SDS-PAGE analysis.
745 The beads were then washed with 3 vol 0.2% SDS. Enriched proteins were eluted by boiling with
746 2% (v/v) 2-mercaptoethanol-containing NuPAGE®LDS sample loading buffer at 95°C for 5 min.
747 Samples were separated by gel electrophoresis.

748 **Gel electrophoresis and in-gel fluorescence**

749 SDS-PAGE analysis was performed with 12% acrylamide Bis-Tris gels, using a BioRad Mini-
750 PROTEAN® Tetra Cell system with MOPS running buffer (5 mM MOPS pH 7.7, 50 mM Tris Base,
751 0.1% SDS, 1mM EDTA), using Precision Plus Protein All Blue Standard (BioRad) as a molecular
752 weight marker. IGF was detected (excitation wavelength 552 nm, emission wavelength 570 nm)
753 using a Typhoon FLA 9500 Imager (GE Healthcare). Further data analysis was performed with
754 ImageQuant software.

755 **Photoaffinity Labelling for nLC-MS/MS**

756 **Probe 2 Treatment of Live *P. falciparum* Gametocytes**

757 For identification (**Figures 1A-B, S1B-C**) and validation (**Figures 1C-F, S2, S3**) of N-4HCS cellular
758 targets by photoaffinity labelling, live *P. falciparum* NF54 stage V gametocyte cultures (\geq 0.3%
759 exflagellation) were treated and irradiated by UV, as opposed to the lysate-based treatment
760 outlined above. For nLC-MS/MS, gametocytes were treated with either DMSO, probe **2** (10 μ M)
761 only or a combination of probe **2** (10 μ M) and parent molecule **1** (10 μ M). DMSO concentration
762 was normalised across all samples and samples were obtained in triplicate. Following treatment,
763 parasites were incubated for 10 minutes at 37°C and subsequently irradiated with UV light at 254
764 nm for 10 minutes. Gametocytes were then purified using Nycoprep™ 1.077 and saponin lysed to
765 lyse erythrocytes. Lysis buffer (1% Triton-X100/10mM Tris/150mM NaCl/cOmplete™ ULTRA
766 EDTA-free Protease Inhibitor Cocktail at pH 7.5 in H₂O) was added to treated gametocyte pellets
767 and parasites were lysed by sonication (60% amplitude, 3 min, (2 s pulse, 2 s rest)) and
768 centrifugation (17,000 x g, 4°C). The supernatant was retained, and probe **2**-labelled proteins were
769 ligated to AzTB by performing the CuAAC reaction as described above.

770 **Pulldown for nLC-MS/MS**

771 Samples being prepared for nLC-MS/MS analysis were incubated with Neutravidin Agarose beads,
772 which produce a low background signal. For bead derivatisation, beads were centrifuged at 7000
773 rpm for 4 min at RT before washing 5 times with triethylammonium bicarbonate (TEAB, 100 mM,
774 pH 8). Beads were then gently agitated for 1 hour at RT in a solution of 100 mM TEAB, 25 mM
775 NaBH₃CN and 0.2% formaldehyde. The reaction was quenched by washing twice with 1%

776 ethanolamine in 100 mM TEAB before subsequently washing 3 times with HEPES (50 mM, pH 8).
777 Before addition of protein samples, derivatised beads were washed twice with 0.2% SDS in
778 HEPES (50 mM, pH 8). Air dried protein samples were dissolved in 0.2% SDS in HEPES (50 mM,
779 pH 8), added to beads and shaken for 2 hours at RT. Following incubation, beads were recovered
780 by spinning at 7000 rpm for 4 minutes at RT and the supernatant was removed. Beads were
781 washed twice with 0.2% SDS in HEPES (50 mM, pH 8) and washed a further 4 times with HEPES
782 (50 mM, pH 8).

783 **LysC and Trypsin Digestion**

784 To elute protein from beads, LysC (in 50 mM HEPES, pH 8) was added to samples and incubated
785 for 1 hour at 37°C, using 2 µl LysC per 30 µl of derivatised beads. Samples were centrifuged at
786 6000 rpm 4 min at RT to pellet beads and 50 µl supernatant of samples were retained and
787 combined. Beads were washed with 50 µl HEPES (50 mM, pH 8). TCEP (5 mM) and CAA (10 mM)
788 were added to the combined supernatants and gently agitated 10 min at RT. Trypsin (0.5 µl of 20
789 µg/100ul in HEPES 50 mM, pH 8.3) was added to each sample and incubated overnight at 37°C.

790 **9-plex TMT Labelling**

791 TMT reagents (Thermo Fisher Scientific, MA) were prepared in acetonitrile and added to an equal
792 volume of sample before incubating with moderate shaking for 2 hours at RT. Each reaction was
793 quenched with 1 µl 5% hydroxylamine before combining all samples into one tube. The sample
794 was dried by centrifugal evaporation at 45°C.

795 **Desalting and 3-Layer Fractionation**

796 All fractionation centrifugations were performed at 1,100 x *g* for 2 min at RT. Samples were
797 resuspended in 150 µl 1% (v/v) TFA/H₂O, 90% of sample volume was transferred to a stage tip
798 containing SDB-RPS (polystyrene-divinylbenzene copolymer modified with sulfonic acid, Supelco)
799 and centrifuged. Columns were desalted by washing with 0.2% TFA (60 µl) before elution into
800 separate tubes, with sequential addition of three buffers ([Table S3](#)). Samples were evaporated to
801 dryness in a Savant SPD1010 SpeedVac® Concentrator at 45°C. Prior to separation and analysis
802 by QExactive LC-MS, dried fractionation samples were resuspended in 2% ACN, 0.5% TFA in H₂O

803 (LC-MS grade) by gentle agitation and sonication, to give a final concentration of ~ 1 µg/µl. A stage
804 tip-filter was prepared, containing 3-layers of PVDF Durapore filter (0.1 µm). Samples (12 µl) were
805 transferred to stage tips and centrifuged into LC-MS vials at 2000 rpm for 3 min at RT.

806 **nLC-MS/MS Data Acquisition**

807 Peptides were separated on an Acclaim PepMap RSLC column (50 cm x 75 µm inner diameter,
808 Thermo Fisher Scientific) using a 3-hour acetonitrile gradient in 0.1% aqueous formic acid, at a
809 flow rate of 250 nl/min. Easy nLC-1000 was coupled to a QExactive mass spectrometer via an
810 easy-spray source (Thermo Fisher Scientific). The QExactive was operated in data dependent
811 mode with survey scans acquired at a resolution of 70,000 at m/z 200. Scans were acquired from
812 350 to 1800 m/z. Up to 10 of the most abundant isotope patterns (a minimum of charge 2) from the
813 survey scan were selected with an isolation window of 1.6 m/z and fragmented by HCD with
814 normalised collision energy of 31. The maximum ion injection times for the survey scan and the
815 MS/MS scans (acquired with a resolution of 35,000 at m/z 200) were 20 and 120 ms, respectively.
816 The ion target value for MS was set to 106 and for MS/MS to 2 x 10⁵, and the intensity threshold
817 was set to 1.7 x 10³.

818 **Protein Database Search and TMT-labeling Quantification**

819 Raw files were uploaded into MaxQuant (version 1.6.1.0)⁵⁵ and searched against the curated
820 Uniprot *P.falciparum* NF54 proteome (Uniprot, Feb 2018, 8637 entries)⁵⁶ using the built-in
821 Andromeda search engine. Cysteine carbamidomethylation was selected as a fixed modification,
822 and methionine oxidation and acetylation of protein N terminus as variable modifications. For in
823 silico digests of the reference proteome, the following peptide bond cleavages were allowed:
824 arginine or lysine followed by any amino acid (a general setting referred to as Trypsin/P). Up to two
825 missed cleavages were allowed. The false discovery rate was set to 0.01 for peptides, proteins,
826 and sites. Other parameters were used as pre-set in the software (maximal mass error 4.5 ppm
827 and 20 ppm for precursor and product ions, respectively, minimum peptide length = 7, minimum
828 razor unique peptides = 2, minimum scores for unmodified and modified peptides = 0 and 40,
829 respectively). “Match between runs” option (time window 0.7 min) was allowed and “Unique and

830 razor peptides” mode was selected to allow identification and quantification of proteins in groups
831 (razor peptides are uniquely assigned to protein groups and not to individual proteins), and for TMT
832 quantification (MS2 mode) the minimal ratio count 2 was selected.

833 **Proteomics Data Analysis**

834 Data analysis was performed using Perseus (version 1.6.5.0)⁵⁷. Corrected reporter intensity values
835 were filtered to remove rows based on ‘contaminants’ and ‘reverse’ columns. The data was log₂
836 transformed and the median values within each column (TMT channel) subtracted. Protein groups
837 with at least two valid values were retained. A two-sample t-test (Permutation-based FDR = 0.10;
838 S0 = 0.15) was applied to all proteins in the dataset and results analysed according to their
839 statistical significance.

840 **TARGET VALIDATION**

841 **Photoaffinity labelling analysed by in-gel fluorescence and western blot**

842 **Treatment and copper catalysed azide-alkyne cycloaddition**

843 For in-gel fluorescence and western blot analysis (**Figures 1C-F, S2, S3**), live *P. falciparum* NF54
844 gametocytes were treated with either DMSO or probe **2** (2.5 µM, 5 µM or 10 µM) and irradiated
845 described above. Gametocytes were purified with Nycoprep 1.077 and saponin lysed to obtain a
846 parasite pellet. The pellets were lysed by sonication (60% amplitude, 3 min, (2 s pulse, 2 s rest))
847 and centrifuged (17,000 g, 4°C) in lysis buffer (1% Triton-X100/10mM Tris/150mM
848 NaCl/cOmplete™ ULTRA EDTA-free Protease Inhibitor Cocktail at pH 7.5 in H₂O).

849 Protein concentration was determined using the Pierce™ BCA Protein Assay Kit following the
850 manufacturer’s instructions. Absorbance was measured using a NanoDrop™ 2000
851 spectrophotometer, using BSA as a protein standard. Lysed protein was made up to 0.5-1 mg/ml in
852 PBS to a volume of 100 µl to perform the CuAAC reaction and protein precipitation, as described
853 above. Samples of the clicked sample and crude lysate, with a total of 10 µg protein each, were set
854 aside to be analysed by in-gel fluorescence and western blot.

855 **Pulldown and IGF**

856 Following CuAAC, protein samples were incubated with Pierce™ streptavidin coated magnetic
857 beads, using 300 µL beads per 1 mg of total protein. Beads were washed 3 times by moderately
858 shaking with 0.2% SDS in PBS and partitioning with a magnet. Protein samples were added to the
859 washed beads and incubated at RT for 2 h, with moderate shaking. The flow-through was retained
860 for analysis by partitioning with a magnet and beads were then washed 3 times with 0.2% SDS.
861 Beads were washed once more with 0.1% Tween-20 in H₂O before addition of 0.1 M glycine, pH
862 2.0 and moderate shaking for 5 min at RT. Enriched proteins were then boiled with 2 x sample
863 loading buffer for 10 min at 95°C before centrifuging (17,000 x *g*, 10 min at RT). The resulting
864 eluate was loaded directly onto an SDS-PAGE gel additionally to flow-through, crude lysate and
865 clicked samples.

866 Proteins were separated on NuPage 4-12% Bis-Tris gels (Novex) and TAMRA IGF was detected
867 with a FLA 5000 biomolecular imager. Gels were further analysed by Western blot using standard
868 methods, developed using ECL (Amersham). Pfs16 was detected with 1:800 mouse anti-Pfs16
869 clone 32F717:B02⁵⁸, kindly donated by Robert Sauerwein and colleagues, or 1:2000 rabbit anti-
870 Pfg377⁵⁹, kindly donated by Tomoko Ishino and colleagues. Secondary antibodies Goat anti-rabbit
871 or goat anti-mouse horseradish peroxidase (HRP) were used at a 1:10,000 dilution.

872 **CETSA**

873 The melt curve and isothermal dose response (ITDR)-CETSA protocols were adapted from
874 previously described protocols³⁴. An immunoblot-based approach was carried out with activated
875 gametocyte or mixed stage I-III/asexual parasite lysate. The soluble protein fraction of parasites
876 pellets was obtained by addition of lysis buffer (1% Triton-X100/10mM Tris/150mM
877 NaCl/cOmplete™ ULTRA EDTA-free Protease Inhibitor Cocktail at pH 7.5 in H₂O) and
878 centrifugation at 17,000 x *g* for 20 min at 4°C.

879 To obtain a melt curve for *T_m* extrapolation, the soluble protein fraction was treated with 1% DMSO
880 or 100µM **DDD01035881**. 10µl aliquots of the protein fractions were aliquoted into PCR tubes and
881 incubated at RT for 3 minutes. The fractions were then thermally challenged over a temperature
882 gradient from either 51.6, 76.6, 61.9 or 71.5-100°C for either 5 using the BioRad C1000 Touch™

883 Thermal Cycler and incubated for a further 3 minutes at 4°C. To remove the aggregated proteins,
884 the soluble fraction of the heat-treated parasites was obtained by centrifugation. The stabilised
885 proteins were then prepared for visualisation by immunoblot.

886 The isothermal dose response format of CETSA was performed over a range of concentrations
887 and single temperature of 78.4°C. The temperature was derived from the melt curve as a
888 temperature at which Pfs16 had mostly aggregated under DMSO treatment but was stabilised by
889 **DDD01035881**. **DD01035881** was dispensed into 384 well plates using the HP D300 Digital
890 Dispenser from 1 nM to 100 µM. 10 µl soluble protein, prepared as described above, was added
891 and incubated with **DDD01035881** for 10 minutes. Treated protein was thermally challenged at
892 78.4°C for 5-minute and incubated at 4°C for 3 minutes. The stabilised proteins were then isolated
893 from these fractions by centrifugation and prepared for immunoblot analysis.

894 Gel electrophoresis and detection of Pfs16 and Pfg377 by immunoblot was performed as
895 described above. Densitometry analysis was carried out using ImageJ and data was normalised to
896 the lowest and highest values to obtain relative band intensities. Normalised data was analysed to
897 obtain melt curves using the Boltzmann Sigmoid equation in GraphPad Prism. ITDR data was fitted
898 using the saturation binding curve (one site binding rectangular hyperbola) function in GraphPad
899 Prism.

900 **Flow cytometry measure of sexual conversion**

901 Sexual conversion rates of *Pf*2004/164-tdTomato parasites was determined as previously
902 described³⁶. Asexual parasites with >2% ring-stage parasitemia were synchronised with 5%
903 sorbitol to bring parasites to a window of 0-24 hours post invasion (h.p.i.). Parasites were brought
904 to an 8-hour window (16 to 24 h.p.i) by repeating the synchronisation within the same
905 intraerythrocytic developmental cycle. Synchronised parasites were washed with fresh media,
906 diluted to 2.5% haematocrit and 220µl of dilute cell suspension was plated into the wells of a 96-
907 well plate, for induction of sexual conversion.

908 25µM of **DDD01035881** and derivatives (**DDD01028076**, **(-)-DDD01028076** and **(+)-**
909 **DDD01028076**) and DMSO controls were included across the plate, all wells were normalised to

910 0.25% DMSO. For carryover samples, compounds were plated prior to induction. For post-
911 induction treated samples, compounds were plated 24h after initial plating and induction. For
912 compound washout samples, parasites were plated onto compound treated plates and washed
913 three times at 24 hours-post induction. Parasite controls were included by washing and plating
914 synchronised parasites with media treated with 20µM choline to block sexual conversion.

915 48 hours after induction, the parasitemia of samples was determined by staining 10µl of each
916 sample with Sybr Green (1:5000 in PBS). Cells were stained for 20 minutes at 37°C and washed
917 twice before measuring Sybr Green positive cells as a measure of parasitemia by flow cytometry
918 using a BD Fortessa flow cytometer. Sybr Green was detected with the 488 nm laser using the
919 530/30 filter and tdTomato with the 561 nm laser using the 586/16 filter. 100,000 events were
920 acquired per sample. 48 hours after counting parasitemia, Sybr Green staining was repeated to
921 measure gametocytaemia by flow cytometry. Sybr Green and tdTomato double positive cells
922 represented gametocyte populations. 400,000 events were acquired per sample.

923 The sexual conversion rate of each sample was determined with the following equation:

$$\text{Sexual conversion rate} = \frac{\text{gametocytemia}}{\text{parasitemia 48h post induction}}$$

924 **Relative exflagellation counts**

925 For incremental compound treatment post-gametogenesis, 5 parts of stage V NF54 gametocytes
926 (day 14 post-induction and onwards) were activated with 1-part ookinete medium at RT. Cells were
927 treated with varying concentrations of **DDD01035881**, ML10, 1294 at time increments post-
928 activation. Viability was then determined by counting exflagellation events or cells were prepared
929 for imaging. For viability measurements, exflagellation rates relative to erythrocyte density were
930 determined at 25 minutes post-activation using a haemocytometer. For immunofluorescence
931 labelling, cells were fixed at 25 minutes post-activation and stained as described above.

932 To determine reversibility of **DDD01035881**, gametocytes were activated as described above and
933 compound was removed with 3 washes at 1 or 6 min post-activation. Viability was determined by
934 counting exflagellation rates at 25-minutes post-activation. Exflagellation rates of **DDD01035881**-

935 treated gametocytes was determined relative to DMSO controls. Relative rates of **DDD01035881**-
936 treated parasites which were washed at 1 or 6 minutes were calculated relative to DMSO controls
937 which were washed three times at 1-minute post-activation, accounting for reductions in
938 exflagellation due to centrifugation.

939 **Flow cytometry measure of microgametocyte ploidy**

940 The extent of DNA replication of *PfDynGFP/P47mCherry* gametocytes with and without
941 **DDD01035881** treatment was determined as previously described⁶⁰. Stage V
942 *PfDynGFP/P47mCherry* and NF54 gametocytes were purified with NycoPrep™ 1.077. Purified
943 gametocytes were resuspended in suspended activation medium (RPMI-1640 with 25mM HEPES
944 (Life Technologies), 4mM sodium bicarbonate, 5% fetal bovine serum, pH 7.20) to permit staining
945 at RT without premature activation of gametogenesis. For T=15 min samples, parasites were
946 activated with ookinete medium and gametogenesis was halted with ice cold PBS at 15 minutes.
947 For T=0 min samples, parasites were immediately resuspended in ice cold PBS. All samples were
948 washed at 300g for 2 min at 4°C, resuspended in ice cold PBS and stained with 1:2000 Vybrant™
949 DyeCycle™ Violet (Thermo-Fisher) for 30 min at 4°C. Stained and unstained erythrocyte and NF54
950 (T=0 and T=15 min) controls were prepared. DNA content was measured as Vybrant™
951 DyeCycle™ Violet intensity by flow cytometry and data was analysed using FlowJo software. GFP
952 positive male gametocytes were gated and ploidy was measured and expressed as a percentage
953 of the total male population. The 530/30, 610/10 and 450/50 filters were used to analyse GFP,
954 mCherry and Vybrant DyeCycle™ Violet, respectively. 100,000 events were analysed per sample.

955 **Immunofluorescence staining and imaging**

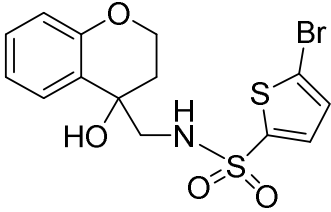
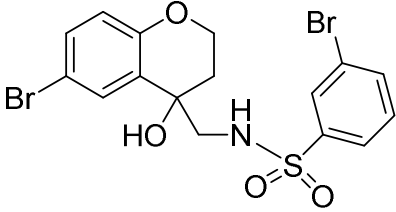
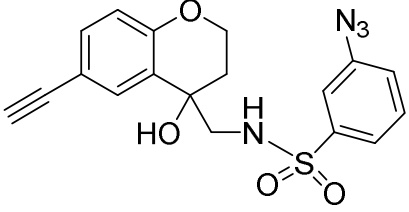
956 Mature NF54 gametocyte culture was treated with either DMSO or test compounds. Gametocytes
957 were treated with 5µM **DDD01035881**, 1µM 1294 and 25µM ML10, before immediately activating
958 without prior incubation. Gametocytes were treated with 50µM Colchicine and Cytochalasin B for
959 48 hours. For T=0 samples, compounds were immediately fixed in prewarmed 4%
960 paraformaldehyde. Cultures were activated by xanthurenic acid-containing ookinete medium and
961 fixed at increments post-activation. All fixed samples were adhered to poly-L-lysine (Sigma) coated

962 glass coverslips, before cells were washed once in PBS, permeabilised in 0.1% Triton-X100,
963 washed thrice more in PBS and blocked with 10% fetal bovine serum. Cells were labelled with
964 primary antibodies for 1 hour; 1:500 mouse anti-alpha tubulin clone DM1A (Sigma), 1:1000 rabbit
965 anti-Glycophorin A clone EPR8200 (Abcam) and 1:800 mouse anti-Pfs16 clone 32F717:B02⁵⁸ (a
966 kind gift from Robert Sauerwein, Radboud University Medical Centre). Cells were labelled with
967 secondary antibodies and other stains for 45 minutes; 1:500 anti-mouse or anti-rabbit Alexa Fluor
968 488 (Thermo-Fisher), anti-mouse or anti-rabbit Alexa Fluor 594 (Thermo-Fisher), 5µg/ml Wheat
969 Germ Agglutinin (WGA)-633 and 10nM 4',6-diamidino-2-phenylindole (DAPI). VectaShield
970 mountant (Vector Laboratories) was used to mount coverslips onto glass slides. Images were
971 acquired with a Nikon Ti-E inverted widefield microscope at x100 objective in 0.2 µm increments
972 through Z, using NIS Elements v4.20. Z-stack images were deconvolved using the EpiDemic
973 plugin and compressed to maximum intensity projections in Icy Bioimage Analysis software.

974 **Electron Microscopy**

975 Stage V NF54 gametocytes were purified by density barrier isolation with NycoPrep[®] 1.077.
976 Purified gametocytes were treated with either DMSO or 5µM **DDD01035881** prior to activation with
977 ookinete medium. Parasites were fixed at 25 min post-activation with 4% high EM grade PFA/2.5%
978 v/v glutaraldehyde/ 0.1% tannic acid in 0.1 M sodium cacodylate buffer pH 7.2 for 3 hrs at RT and
979 washed three times in cold 0.1 M sodium cacodylate buffer at 20 min intervals. Cells were treated
980 with 1% w/v osmium tetroxide in 0.1 M sodium cacodylate for 2 hrs at room temperature (RT),
981 washed with 0.1 M sodium cacodylate and stained with 1% w/v aqueous uranyl acetate for 1 hr at
982 RT. Samples were then dehydrated in an ethanol series and embedded in epoxy resin (TAAB). 70
983 nm sections were cut using a Leica EM UC7 ultramicrotome, contrasted with Uranylless (TAAB) for
984 2 min and with 3% Reynolds lead citrate (TAAB) for 1 min according to the manufacturer's
985 protocols. Sections were imaged on a JEOL JEM-1400Plus TEM (120 kV) with a Ruby Camera (2
986 K × 2 K).

987 **FIGURES**

Structure	Compound	Male IC ₅₀ (nM)
	DDD01035881	292±76
	1	785±48
	2	3981±211

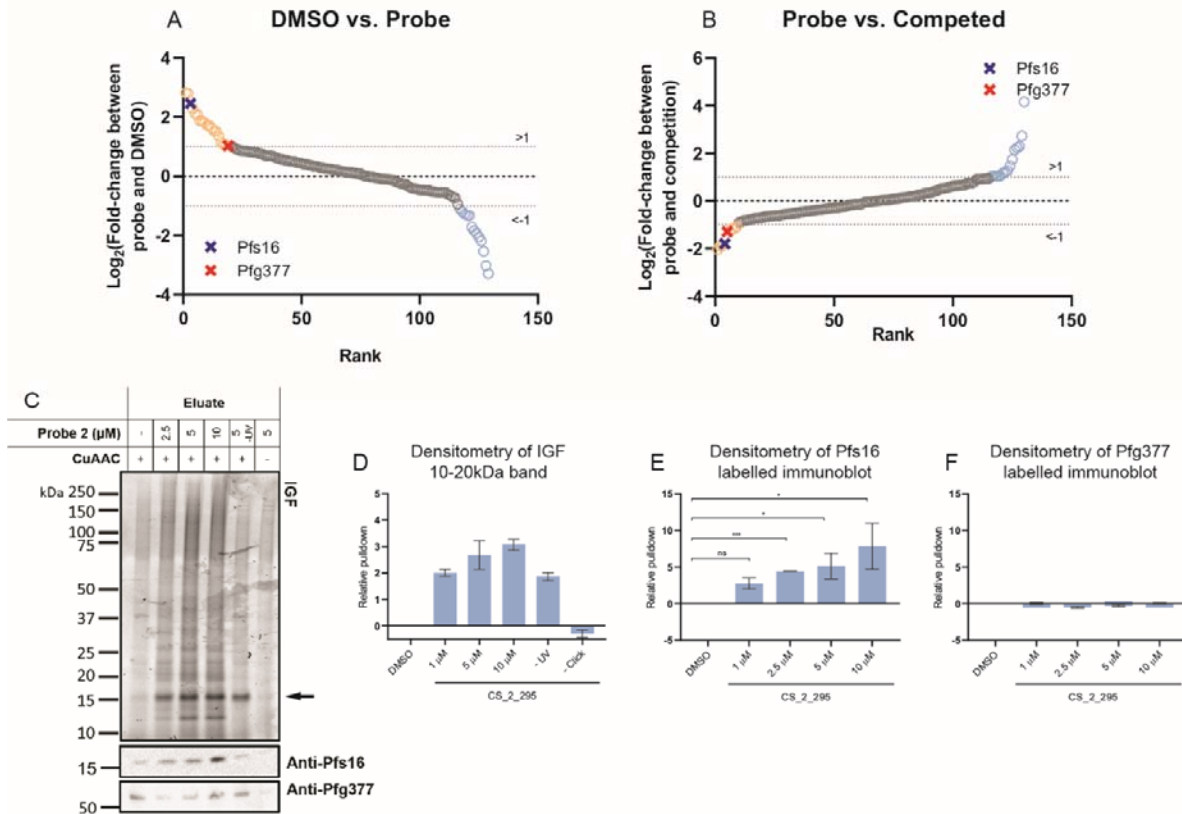
988

989 **Table 1. DDD01035881 and derivatives**

990 Activity of **DDD01035881** and structural analogues as determined in a structure activity relationship
991 study. IC₅₀s depicted represent the inhibition of male gamete viability as determined by the male
992 gamete formation format of the DGFA. Values are expressed as an average ± SEM of 3-8
993 biological replicates, ≥ 2 technical replicates.¹⁵

994

995



996

997 **Figure 1. Identification and validation of Pfs16 as a specific interaction partner with the N-**
 998 **4HCS series**

999 ⁶¹ Results of *P. falciparum* proteome-wide target identification study. Proteins enriched by PAL and
 1000 pulldown were identified by nLC-MS/MS. Plots depict the log₂-transformed fold change in protein
 1001 enrichment between the of **(A)** DMSO and probe **2** treated samples or **(B)** probe **2** and competition
 1002 (combined treatment probe **2** and parent molecule **1**) samples. All protein hits, represented as
 1003 circles, are ranked based on the log₂-transformed fold change in enrichment, between the average
 1004 values of samples. Averages were taken of 3 distinct biological replicates. Orange circles denote
 1005 positive log-transformed fold change >1 and blue circles denote negative log-transformed fold
 1006 change <-1 in **A**, and vice-versa in **B**. Pfs16 and Pfg377 are marked with blue and red circles,
 1007 respectively, in both **A** and **B**. Hits enriched in both conditions are listed in **Table 2**. **(C-F)**
 1008 Validation of Pfs16 and Pfg377 binding by live probe **2** treatment, AzTB conjugation, streptavidin-
 1009 biotin affinity enrichment and analysis by IGF and immunoblot. IGF fluorescence was used to
 1010 identify streptavidin-enriched proteins and corresponding immunoblots validated the specificity of

1011 pulldowns to Pfs16 and Pfg377. **(C)** IGF revealed an abundantly TAMRA-labelled protein between
1012 15kDa and 20kDa in size, likely corresponding to Pfs16. Band intensity, relative to DMSO, is
1013 depicted as an average and error bars denote SEM of 3 biological replicates. See **Figure S2B-C**
1014 for further replicates. **(D)** Densitometry of the 16kDa protein band in **C** and **Figure S2B-C** was
1015 determined and is depicted as relative band intensity relative to a DMSO control in the presence of
1016 increasing probe **2** concentration. Values depict averages and error bars denote SEM of 3
1017 biological replicates. Densitometry of corresponding immunoblots labelled with **(E)** Pfs16 and **(F)**
1018 Pfg377 are depicted as band intensities relative to a DMSO control, in the presence of increasing
1019 probe **2** concentration. Error bars denote SEM of 3 biological replicates, see **Figure S2** for
1020 immunoblots and gels which were analysed to obtain **(D-F)**. Significance was determined by
1021 performing an unpaired two-tailed t-test and is denoted as *** ($p < 0.001$), * ($p < 0.05$) and ns ($p \geq$
1022 0.05).

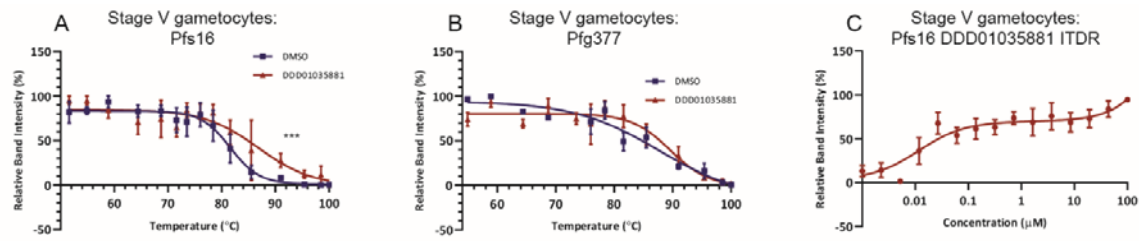
1023

Rank	DMSO vs. probe 2				Probe 2 vs. competition (probe 2 + parent molecule 1)			
	Colloquial Name	Protein ID	Log ₂ FC	P value	Colloquial Name	Protein ID	Log ₂ FC	P value
1	*Pfs16	PF3D7_0406200.1-p1	2.45809	0.0701	Spermidine Synthase	PF3D7_1129000.1-p1	-2.0397	0.1552
2	Spermidine Synthase	PF3D7_1129000.1-p1	2.27369	0.1058	60S Ribosomal Protein L26	PF3D7_0312800.1-p1	-1.8946	0.0051
3	RAB-1B (Ras related protein)	PF3D7_0512600.1-p1	2.08532	0.0314	RAB-1B (Ras related protein)	PF3D7_0512600.1-p1	-1.8675	0.0177
4	60S Ribosomal Protein L26	PF3D7_0312800.1-p1	1.71633	0.0423	*Pfs16	PF3D7_0406200.1-p1	-1.7926	0.3069
5	V-type Proton ATPase	PF3D7_1311900.1-p1	1.34692	0.0567	**Pfg377	PF3D7_1250100.1-p1	-1.2868	0.1180
6	**Pfg377	PF3D7_1250100.1-p1	1.02634	0.4615	V-type Proton ATPase	PF3D7_1311900.1-p1	-1.1617	0.0201

1024

1025 **Table 2. List of protein hits enriched by PAL and nLC-MS/MS**

1026 Protein hits identified as specific to the probe 2-protein interaction profile, including *Pfs16 and
 1027 **Pfg377, ranked according to the log-transformed fold change (Log₂FC) in protein enrichment
 1028 between average values of 3 biological replicates. Proteins depicted were identified as both
 1029 positively enriched when comparing DMSO and probe 2, and, negatively enriched when comparing
 1030 probe 2 and a combination of probe 2 and parent molecule 1. P values listed are derived from
 1031 analysis by student's *t*-test, see **Supporting Information**.

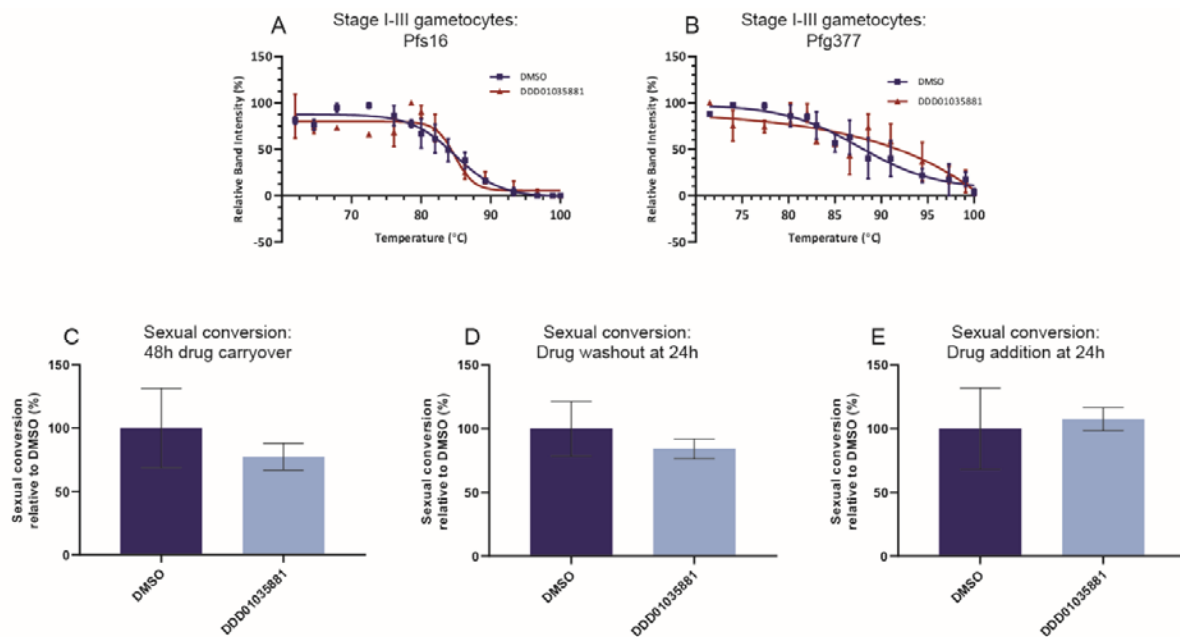


1032

1033 **Figure 2. Label-free validation of Pfs16 interaction with DDD01035881 in mature**
1034 **gametocytes**

1035 **(A-C)** Target validation by CETSA, using densitometric analysis of immunoblots for melt curve
1036 generation and subsequent quantification of T_m. Melt curves demonstrating thermal stability of **(A)**
1037 Pfs16 and **(B)** Pfg377 using activated stage V gametocyte lysate treated with DMSO or
1038 **DDD01035881**. Error bars represent the SEM of 2-3 biological replicates. In **(A)**, a statistically
1039 significant difference was found at 91°C using an unpaired two-tailed t-test ($p < 0.001$). **(C)** The
1040 corresponding isothermal dose response (ITDR) curve of **(A)** depicting the concentration
1041 dependent stabilisation of Pfs16 by **DDD01035881** in activated stage V gametocyte lysate. Error
1042 bars represent the SEM of 4 biological replicates. Full immunoblots can be found in **Figure S4**.

1043



1044

1045 **Figure 3. Effect of N-4HCS series on gametocytogenesis**

1046 Elucidation of the effect of the N-4HCS series on immature gametocytes by CETSA and **(C-E)**

1047 sexual conversion rate calculations. Label-free validation of the effect of **DDD01035881** treatment

1048 to sexual conversion by CETSA was performed on lysate derived from stage I-III gametocytes,

1049 looking specifically at the stabilisation of **(A)** Pfs16 and **(B)** Pfg377. No statistically significant

1050 stabilisation of either Pfs16 or Pfg377 was found at any given temperature between DMSO and

1051 **DDD01035881**. Error bars represent the SEM of 2-3 biological replicates. Full immunoblots can be

1052 found in [Figure S4](#). **(C-E)** The sexual conversion rate of Pf2004/164-tdTomato parasites was

1053 determined by quantification of tdTomato expression after induction of gametocytogenesis.

1054 Conversion rates of **DDD01035881**-treated parasites are expressed as rates relative to the

1055 conversion rates of DMSO-treated parasites. Perturbations to sexual conversion were determined

1056 by **(F)** maintaining treatment over two intraerythrocytic cycles and **(G)** the reversibility of any

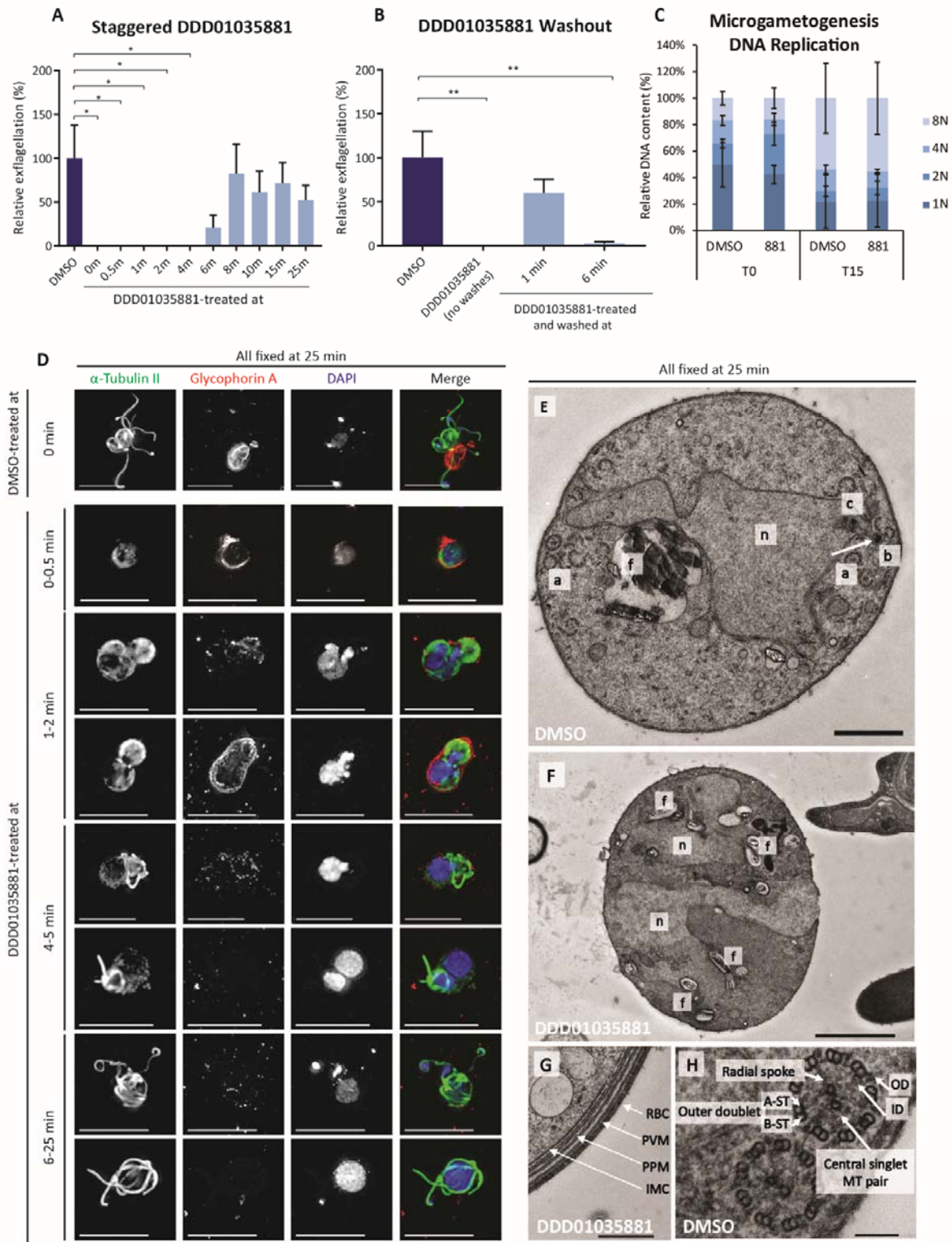
1057 perturbations were determined by removing compound at 24 hours. **(H)** Perturbations to early

1058 gametocyte development were probed by administration of compounds in a subsequent

1059 intraerythrocytic cycle. Error bars represent the SEM of 2 biological replicates. See [Figure S5](#) for

1060 the gating strategy and conversion rates of further N-4HCS analogues.

1061



1062

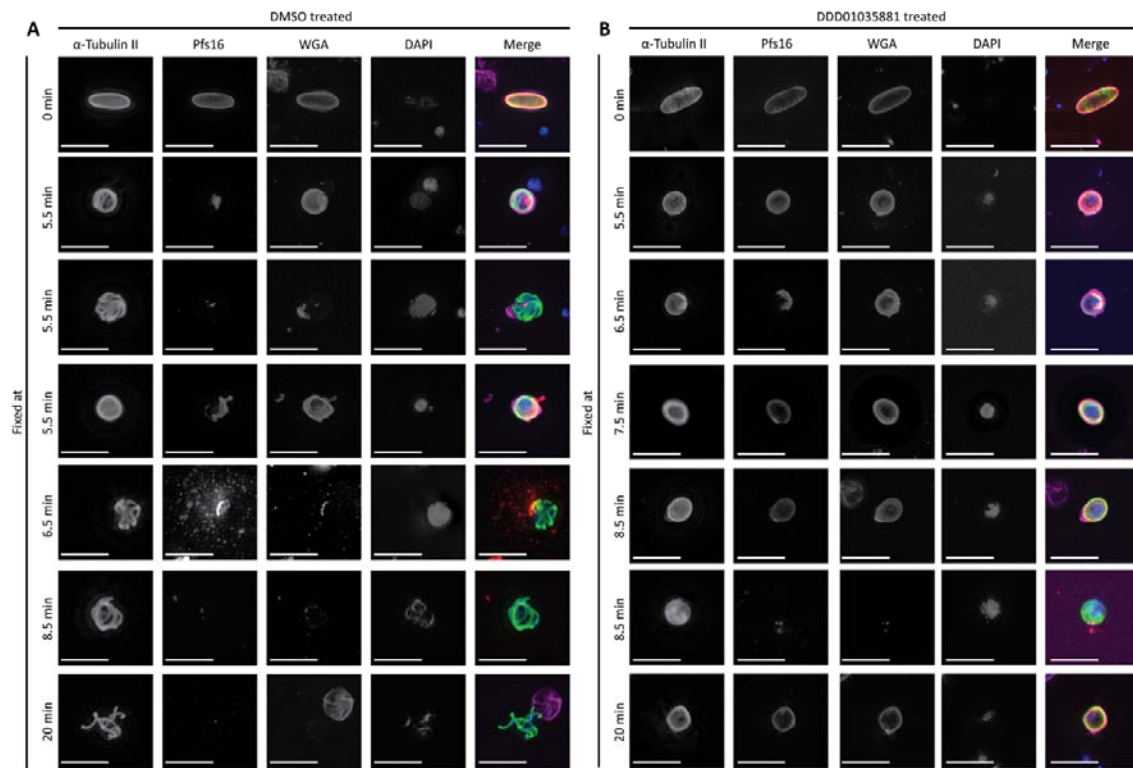
1063 **Figure 4. Microgametogenesis phenotype under DDD01035881 treatment**

1064 Exflagellation rates of gametocytes relative to DMSO controls which were either (A) activated in
 1065 the absence of drug, then treated with 5 μ M DDD01035881 at the stated time points or (B) treated

1066 with **DDD01035881** or DMSO, then activated and washed three times to remove compound at the
1067 labelled time-points (or left under **DDD01035881** pressure without washing). Exflagellation was
1068 counted at 25 minutes and error bars represent the SEM of 5-6 biological replicates. Significance
1069 was determined with an unpaired two-tailed t-test and is denoted as * ($p < 0.05$) and ** ($p < 0.01$).
1070 **(C)** Relative DNA content of *PfDynGFP/P47mCherry* male gametocytes treated with either DMSO
1071 or **DDD01035881** (denoted by 881) at 0 min and measured at 0 and 15 minutes post-activation.
1072 Ploidy of parasites (1n, 2n, 4n or 8n) was determined by flow cytometry as a measure of Vybrant™
1073 DyeCycle™ intensity. Error bars represent the SEM of 3 biological replicates. **(D-H)** Morphological
1074 phenotype of **DDD01035881** treated parasites as determined by fluorescence and electron
1075 microscopy. **(D)** IFAs of abhorrent DDD0103588-treated male gametocytes, depicting alpha
1076 tubulin-labelled cytoskeleton (green), glycophorin A-labelled erythrocyte (red) and DNA (blue).
1077 Parasites were treated at the stated time points relative to activation of microgametogenesis and
1078 fixed at 25 minutes post-activation, the timepoint at which DMSO treated control parasites
1079 exflagellate. Scale bars = 10µm. **(E-H)** EM images of gametocytes treated with **DDD01035881** or
1080 DMSO and then activated and fixed at 25 minutes. **(E)** A DMSO-treated male gamete preparing for
1081 emergence from the gametocyte cell body. The kinetosomal sphere and granule and kinetosomal
1082 basket (b) located at the centriolar plaque within the nucleus (n) which bears an intranuclear
1083 spindle (s) and chromatin (c). The food vacuole (f) near to the nucleus. Both normal and aberrant
1084 9+2 axoneme arrangement (a) at the periphery of the cell, preparing for axoneme emergence from
1085 the cell body. Scale bar = 1µm. **(F)** **DDD01035881**-treated microgametocyte with a disturbed
1086 nuclear structure (n) and food vacuoles (f). Scale bar = 2µm. **(G)** **DDD01035881**-treated
1087 microgametocyte which has failed egress from the host erythrocyte, displaying an intact 4-layer
1088 membrane. Scale bar = 500nm. **(H)** The characteristic 9+2 arrangement of microtubules. A and B
1089 subtubule pairs are spaced apart from the central singlet microtubule (MT) pair using radial
1090 spokes. Scale bar = **100nm**.

1091

1092



1093

1094 **Figure 5. Pfs16 localisation during microgametogenesis with and without DDD01035881**
1095 **treatment**

1096 An IFA time course of microgametogenesis displaying the localisation of PVM protein, Pfs16, as
1097 parasites egress from host cells via the inside-out mechanism. Individual channels are displayed
1098 on the left of all merged channels, displaying alpha-tubulin (green), erythrocyte membrane (pink),
1099 Pfs16 (red) and DNA (blue). Scale bars = 10 μ m. **(A)** DMSO treated gametocytes. As the PVM
1100 prepares to disintegrate prior to erythrocyte egress, Pfs16 either caps or gathers at a pore on the
1101 parasite surface at 5.5 minutes post-activation. At the point of egress, the capped or pore-localised
1102 Pfs16 vesiculates and bursts at the surface of the parasite at around 6.5 minutes. Beyond the point
1103 of PVM and erythrocyte egress, Pfs16 is absent from the parasite. **(B)** **DDD01035881** treated
1104 gametocytes demonstrate a mixed phenotype, with populations of male gametocytes either failing
1105 to or successfully egressing from the host cell. Parasites which fail to egress demonstrate continual
1106 Pfs16 localisation to the PVM across the entire time course. Parasites which do egress from the
1107 host cell demonstrate capping of Pfs16, but Pfs16 does not form a pore, vesicles or burst from the
1108 PVM.